Interference Mitigation in Feedforward Opportunistic Communications

Jordi Borras, *Member, IEEE*, and Gregori Vazquez, *Senior Member, IEEE*

***Abstract*—This paper deals with scenario-aware, uncoordinated, and distributed signaling techniques in the context of feedforward opportunistic communications, that is, when the opportunistic transmitting node does not cooperate with any other node in a heterogeneous communication context. In this signaling technique, each network node individually follows a transmission strategy based on the locally sensed occupied and unused physical-layer network resources to minimize the induced interference onto other coexisting networks, taking into account the impact of the sensing errors and the locality of the sensing information. The paper identifies and characterizes critical invariance properties of the transmitted pulse shaping waveforms that guarantee the detectability of the feedforward transmitted signal by the uncoordinated receiving nodes, irrespective of the sensing signal space basis. The paper also shows that, under mild operating conditions, the proposed transmission scheme asymptotically defines efficient alternatives in the frequency domain, such as the circulant-shaping TDMA (CS-TDMA) modulation, and all of them admit a direct adaptation to frequency-selective channels. Numerical evaluation of the proposed schemes validates the provided theoretical models.**

***Index Terms*—Feedforward opportunistic communications, uncoordinated distributed communications, noncooperative communications, context-aware waveform design, interference mitigation.**

I. Introduction

INTERFERENCE management plays a fundamental role in multi-user networks to permit the coexistence of several transmitter-receiver pairs sharing the same network resources. While the problem of interference management has been widely studied in coordinated or cooperative networks, the most challenging uncoordinated or non-cooperative case is still an open field [3].

Regarding the cooperative case, the transmitting/receiving nodes can cooperate with each other to equivalently form network multiple-input multiple-output (MIMO) systems, where coordinated multi-point [4] or MIMO broadcast [5] schemes can be implemented. Another interesting strategy is interference alignment (IA) [6], [7], which can be optimal at high signal-to-noise ratio (SNR) regimes. Nevertheless, IA-based schemes have three main limitations [8]: (i) all coexisting terminals have to be involved in the alignment, (ii) the provided gains at low-to-moderate SNR regimes are limited, and (iii) the need for full channel state information (CSI) at all transmitters. In fact, the necessity of CSI at transmitters is a common factor in most interference management strategies. Several works, e.g. [9], study the impact of not exploiting CSI at transmitters but still require user cooperation. Cooperation between coexisting transmitter-receiver pairs to jointly design transmitting-receiving strategies can significantly improve the system performance up to known limits. Notably, [10] reveals that an interference-limited network cannot turn into a noise-limited one. Besides, in heterogeneous networks, where different communication technologies coexist, achieving full user cooperation can be either prohibitive or unrealistic.

In this sense, opportunistic communication [11]–[14] refers to adaptively using the sensed available network resources trying to avoid inducing inter-system interference on the other network nodes. A classical strategy to avoid interferences in opportunistic communications involves steering the opportunistic transmissions to the so-called network null space. Although a rigorous mathematical definition is further given in the paper, at this point, in a broad sense, null space stands for the set of unused physical-layer network resources. Despite null-space communication strategies have been widely used in interweave systems [15], they have also been recently used to improve the interference cancelation performance in the context of rate-splitting multiple-access [16], and to avoid interference between coexisting technologies in ultra-reliable low-latency communications [17] and integrated sensing and communications methods [18].

Opportunistic multi-antenna nodes can exploit the null space of cross-interference channels through beamforming or linear precoding as in [19], or through opportunistic IA [20]–[22] that permits exploiting additional dimensions left over due to the power allocation policy employed by active transmitters. Due to their reduced spatial DoF, single-antenna opportunistic nodes have a smaller null space, thus reducing their transmission opportunities and interference mitigation capabilities. In this case, Vandermonde-subspace frequency-division multiplexing (VFDM) [23]–[25] allows single-antenna opportunistic nodes to exploit the null space induced by the frequency-selective nature of the channel and the guard interval, as the cyclic prefix in OFDM systems, employed by the active transmitter-receiver pairs. VFDM has been also extended to multi-user [26] and multi-antenna [27], [28] scenarios.

The major limitations of the reviewed null-space schemes are their lack of robustness to null-space inference errors and the necessity of coordination between opportunistic transmitter and receiver. Regarding the former, the determination of the

This work has been supported by the Spanish Ministry of Science and Innovation through project RODIN (PID2019-105717RB-C22 / MCIN / AEI / 10.13039/501100011033) and fellowship FPI BES-2017-080071.

The authors are with the Department of Signal Theory and Communications of the Technical University of Catalonia (UPC), 08034 Barcelona, Spain. E-mail: {jordi.borras.pino, gregori.vazquez}@upc.edu

Preliminary results have been presented at 2019 IEEE International Conference on Communications [1] and 2019 IEEE Global Communications Conference [2].

null space has been the focus of a vast amount of literature [29]–[33] (and references therein). It is shown that all these schemes suffer from false-alarm and miss-detection errors, and generally, they are highly conditioned to the local wireless environment. The characterization of these sensing errors is challenging, highly dependent on the adopted method, and not traditionally considered in the reviewed schemes. In this sense, the reviewed schemes assume a *perfect* knowledge of the null space. Regarding the necessity of coordination, feedback-based network consensus is typically used to avoid any inter-node null-space mismatch and agree on a reference system (i.e., basis) for the null space.

The aforementioned limitations motivate the study of robust and non-cooperative interference management strategies. In this sense, the paper studies the distributed design of transmission-reception waveforms robust to the partial or imperfect knowledge of the null space. The paper focuses on opportunistic transmission strategies such that the opportunistic transmitting node does not cooperate with any other node in a heterogeneous communication context, further on referred to as *feedforward opportunistic communication* problem. In this respect, the major contributions of this paper are: (i) investigating the impact and consequences of removing the cooperative feedback between opportunistic nodes in the single-antenna opportunistic communication case, and (ii) including a generalized sensing error model, based on the subspace leakage idea [34], suitable to be adopted in robust null-space communication systems.

In particular, we propose to design opportunistic transmission pulse-shaping waveforms in single-antenna feedforward opportunistic communications under null-space sensing errors, aiming to maximize the worst-case signal-to-interference ratio (SIR) at the opportunistic transmitting node, that is, minimizing the worst-case induced interference by the opportunistic transmitter. This solution generalizes the classic null-space approaches [19]–[28] and is optimal in the inter-system interference sense. In contrast to classic null-space approaches, the proposed solution is *invariant*, i.e. unique, within the given null space, revealing that coherent waveform detection is feasible under ideal operating conditions despite the lack of end-to-end cooperation. Anyhow, the solution is robust to performance losses induced by the inter-node null-space mismatch. Asymptotically, under mild operating conditions, the solution defines a time-multiplexing strategy, named circulant-shaping TDMA (CS-TDMA), which admits an efficient online implementation.

The remainder of this work is organized as follows. Section II describes the signal model and the addressed problem. The general solution and its main properties are analyzed in Section III. Section IV provides the asymptotic behavior and studies the efficient CS-TDMA modulation and the adaptation to frequency-selective channels. The conclusions are drawn in Section V.

Notation: Boldface lowercase (respectively, uppercase) denotes vectors (respectively, matrices). Uppercase calligraphic letters denote a subspace or a set. $(\cdot)^T$, $(\cdot)^*$ and $(\cdot)^H$ denote the transpose, conjugate, and transpose conjugate (Hermitian). $\mathbf{0}_{m\times n}$ and $\mathbf{1}_{m\times n}$ are the $m \times n$ all-zeroes and all-ones matrices. $\boldsymbol{I}_K$ is the $K \times K$ identity matrix. $\langle \boldsymbol{X} \rangle$ refers to the column-space of $\boldsymbol{X}$. $\|\cdot\|_{\mathrm{F}}$ denotes the Frobenius norm. $\odot$ is the Schur-Hadamard product. $\mathrm{mod}\ K$ is the modulo-K operator. $\mathcal{N}_{\mathbb{C}}(\boldsymbol{\mu}, \boldsymbol{\Sigma})$ denotes a complex Gaussian distribution with mean $\boldsymbol{\mu}$ and covariance $\boldsymbol{\Sigma}$.

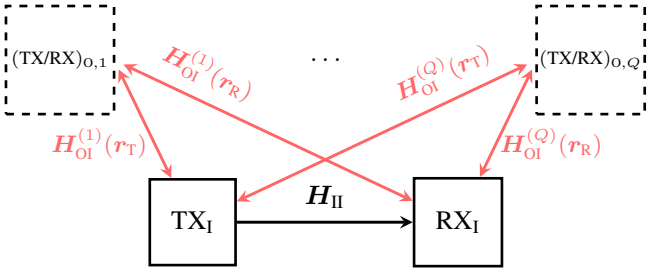

Fig. 1: Inter-system interference problem considered in this work. (TX/RX)$_{\mathrm{O},q}$ represents the q-th outer transmitter-receiver pair, whereas TX$_{\mathrm{I}}$ and RX$_{\mathrm{I}}$ represent the inner transmitter and receiver, respectively. $\boldsymbol{H}_{\mathrm{II}}$ is the inner channel. $\boldsymbol{H}_{\mathrm{OI}}^{(q)}(\boldsymbol{r})$ is the interference channel between the q-th outer-network pair and the inner node located at position $\boldsymbol{r}$, where $\boldsymbol{r} = \boldsymbol{r}_{\mathrm{T}}$ and $\boldsymbol{r} = \boldsymbol{r}_{\mathrm{R}}$ are the position of inner transmitter and receiver, respectively. All the involved channels are unknown by the inner transmitter TX$_{\mathrm{I}}$. All channels are denoted in matrix form for generality, whose size depends on the fading conditions and will be given as needed.

II. Signal Model and Problem Formulation

A. Signal Model

Consider a heterogeneous wireless network[1] composed of an arbitrary number Q of transmitter-receiver pairs that we will refer to as *outer terminals* operating at different rates and with different coded-modulation formats, as depicted in Figure 1. A new asynchronous transmitter-receiver pair, denoted as *inner terminals,* seeks opportunistically accessing the locally sensed available resources while minimizing the caused interference on the outer terminals.

The system coexistence occurs within the bandwidth $[-W/2, W/2]$ and with time-limited signals of duration T. As for in [35], [36, Chapters 2 and 6], the asymptotic total number of complex degrees of freedom (DoF) is $N \approx TW$. Note that N is the size of the set of complex numbers required to specify any particular class of signals in an orthogonal expansion, that is, N is the maximum number of memoryless channel uses under these conditions.

For the sake of generality, we consider that P information blocks have to be transmitted. Each block is composed of K symbols, which are transmitted in parallel through K orthogonal waveforms. The number of orthogonal waveforms K has to be set to satisfy the rate requirements of the inner-network nodes. Accordingly, a total of KP zero-mean and unit-variance independent symbols $a_{k,l}$, for $k = 0, \ldots, K-1$ and $l = 0, \ldots, P-1$, from a given constellation $\mathcal{C}$ are transmitted. At this point of the work, we assume that the channel between the inner nodes is memoryless, that is, the duration N of each block is larger than the channel delay spread. Under a block frequency-flat fading model such that

[1]This paper does not make any assumption about the adopted division duplex scheme, despite time division duplex (TDD) can be a more informative alternative since channel reciprocity holds.

the channel remains constant for N samples, the discrete-time signal model at the inner receiver for the l-th block reads as

$$y_l[n] = \sqrt{\frac{S_{\mathrm{R},l}}{K}} \sum_{k=0}^{K-1} a_{k,l}\phi_k[n - lN] + i_l[n] + w[n], \quad (1)$$

for $n = 0, \ldots, N-1$, where $\phi_k[n]$ are the sampled versions of the transmitted orthonormal pulses $\phi_k(t)$; $S_{\mathrm{R},l} = |h_{\mathrm{II},l}|^2 S_{\mathrm{T}}$ stands for the average received power, being S_{T} the average total transmitted power and $h_{\mathrm{II},l}$ the inner channel coefficient; $i_l[n]$ is an unstructured interference term; and $w[n] \sim \mathcal{N}_{\mathbb{C}}(0, \sigma_w^2)$ is the receiver complex, one-sided, circularly-symmetric Gaussian thermal noise.

Regarding Figure 1, under the block frequency-flat fading assumption, the inner channel matrix $\boldsymbol{H}_{\mathrm{II}}$ is a diagonal matrix given by $\boldsymbol{H}_{\mathrm{II},l} = h_{\mathrm{II},l}\boldsymbol{I}_N \in \mathbb{C}^{N\times N}$. Note that subscript l denotes the assumed block-fading nature of the channel. Moreover, the cross-interference channel matrices $\boldsymbol{H}^{(q)}_{\mathrm{OI},l}(\boldsymbol{r}_{\mathrm{R}})$ are given by $\boldsymbol{H}^{(q)}_{\mathrm{OI},l}(\boldsymbol{r}_{\mathrm{R}}) = h^{(q)}_{\mathrm{OI},l}(\boldsymbol{r}_{\mathrm{R}})\boldsymbol{I}_{N'} \in \mathbb{C}^{N'\times N'}$, being $h^{(q)}_{\mathrm{OI},l}(\boldsymbol{r}_{\mathrm{R}})$ the interference channel coefficients and N' an unknown integer magnitude. The interference term is thus given by $i_l[n] = \sum_{q=1}^{Q} h^{(q)}_{\mathrm{OI},l}(\boldsymbol{r}_{\mathrm{R}})s_q[n]$, which depends on the unknown $h^{(q)}_{\mathrm{OI},l}(\boldsymbol{r}_{\mathrm{R}})$ and the unknown incoming signals from the outer-network terminals $s_q[n]$. Thus, the structure of the interference cannot be exploited by the inner receiver. The frequency-selective channel case is discussed in Section IV.

Focusing on an arbitrary received block l and dropping the index l for notational simplicity, (1) can be vectorized as

$$\boldsymbol{y} = \sqrt{\frac{S_{\mathrm{R}}}{K}} \sum_{k=0}^{K-1} a_k\boldsymbol{\phi}_k + \boldsymbol{i} + \boldsymbol{w} \in \mathbb{C}^N, \quad (2)$$

with $\boldsymbol{\phi}_k = [\phi_k[0], \ldots, \phi_k[N-1]]^T \in \mathbb{C}^N$, $\boldsymbol{i} = [i[0], \ldots, i[N-1]]^T \in \mathbb{C}^N$, and $\boldsymbol{w} = [w[0], \ldots, w[N-1]]^T \in \mathbb{C}^N$. Accordingly, the associated statistic for decoding the k-th received symbol is given by

$$z_k = \boldsymbol{\psi}_k^H \boldsymbol{y}, \ \text{ for } k = 0, \ldots, K-1, \quad (3)$$

where $\boldsymbol{\psi}_k = [\psi_k[0], \ldots, \psi_k[N-1]]^T \in \mathbb{C}^N$ is the k-th receiving filter to be designed.

B. Design Objective

The main objective of this work is twofold. The inner transmitter has to design the transmitting orthonormal pulses $\{\boldsymbol{\phi}_k\}_{0\le k\le K-1}$ that cause minimum inter-system interference to the outer-network nodes, whereas the inner receiver has to design the receiving orthonormal pulses $\{\boldsymbol{\psi}_k\}_{0\le k\le K-1}$ such that $\boldsymbol{\psi}_k$ is the matched filter for $\boldsymbol{\phi}_k$ and, in turn, mitigate the inter-system interference from the outer-network nodes. The challenge is that the inner nodes do not cooperate between them or with the outer-network nodes.

To mitigate inter-system interferences, the orthonormal pulses $\boldsymbol{\phi}_k$ and $\boldsymbol{\psi}_k$ have to lie in the outer-node null space, which has to be learned from the interference channels. In this sense, the interference signal observed by the inner terminal located at positioning coordinates $\boldsymbol{r} = [r_x, r_y, r_z]^T$, that is, either the inner transmitter or receiver, $\boldsymbol{x}(\boldsymbol{r}) \in \mathbb{C}^N$ is given by

$$\boldsymbol{x}(\boldsymbol{r}) = \sum_{q=1}^{Q} \boldsymbol{H}^{(q)}_{\mathrm{OI}}(\boldsymbol{r})\boldsymbol{s}_q + \boldsymbol{v}, \quad (4)$$

where $\boldsymbol{H}^{(q)}_{\mathrm{OI}}(\boldsymbol{r}) \in \mathbb{C}^{N\times N'}$ is the interference channel matrix[2] between the q-th outer transmitter-receiver pair and the inner node located at $\boldsymbol{r}$; $\boldsymbol{s}_q \in \mathbb{C}^{N'}$, with $N' \le N$, are the outer-network transmitted signals; and $\boldsymbol{v} \sim \mathcal{N}_{\mathbb{C}}(\boldsymbol{0}_N, \sigma_v^2\boldsymbol{I}_N)$ is the additive noise. In the sequel, we assume that all information about outer nodes is completely unknown to the inner terminals. Under these conditions, the knowledge about the outer networks is purely statistical, and the null-space information comes from the so-called model order selection [32] based on the eigendecomposition of the autocorrelation matrix $\boldsymbol{R}_{\boldsymbol{xx}}(\boldsymbol{r}) = \mathbb{E}\left[\boldsymbol{x}(\boldsymbol{r})\boldsymbol{x}^H(\boldsymbol{r})\right] \in \mathbb{C}^{N\times N}$ sample estimate.

This paper adopts the common model used by all the classic methods on null-space precoding in (5)–(6). Using the available statistical information, the inner node at position $\boldsymbol{r}$ infers a null-space basis $\widehat{\boldsymbol{U}}_{\mathcal{N}}(\boldsymbol{r}) \in \mathbb{C}^{N\times M(\boldsymbol{r})}$, being $M(\boldsymbol{r})$ the number of DoF sensed as available at the inner node located at position $\boldsymbol{r}$, such that the orthonormal waveforms $\{\boldsymbol{\phi}_k\}_{0\le k\le K-1}$ and $\{\boldsymbol{\psi}_k\}_{0\le k\le K-1}$ satisfy

$$\boldsymbol{\phi}_k = \widehat{\boldsymbol{U}}_{\mathcal{N}}(\boldsymbol{r}_{\mathrm{T}})\boldsymbol{\lambda}_k(\boldsymbol{r}_{\mathrm{T}}), \quad (5)$$

$$\boldsymbol{\psi}_k = \widehat{\boldsymbol{U}}_{\mathcal{N}}(\boldsymbol{r}_{\mathrm{R}})\boldsymbol{\lambda}_k(\boldsymbol{r}_{\mathrm{R}}), \quad (6)$$

where $\boldsymbol{\lambda}_k(\boldsymbol{r}) \in \mathbb{C}^{M(\boldsymbol{r})}$ are the linear combination coefficients defining $\boldsymbol{\phi}_k$ or $\boldsymbol{\psi}_k$. All the classic null-space solutions (cf. [7], [19], [20], [23]–[25]) consider the selection of specific columns of matrix $\widehat{\boldsymbol{U}}_{\mathcal{N}}(\boldsymbol{r})$ by adopting coefficient vectors of the form

$$\boldsymbol{\lambda}_k(\boldsymbol{r}) = [\boldsymbol{0}^T_{m(k)-1} \ 1 \ \boldsymbol{0}^T_{M(\boldsymbol{r})-m(k)}]^T, \quad (7)$$

for $k = 0, \ldots, K-1$, where $m(k) \in \{1, \ldots, M(\boldsymbol{r})\}$ refers to the index of the column vector used in the opportunistic transmission. Since the null-space basis is not unique and the column selection, i.e., the choice of $m(k)$, does not respond to any specific criterion, the solutions to the classic null-space approaches are arbitrary[3], that is, not unique.

In this work, this classical constraint is relaxed, and the coefficient vectors $\boldsymbol{\lambda}_k(\boldsymbol{r})$ are allowed to be generic full vectors to be designed. Even though the latter generalizes the classic null-space solution, a recursive design is required to find the orthonormal waveforms $\{\boldsymbol{\phi}_k\}_{0\le k\le K-1}$ or $\{\boldsymbol{\psi}_k\}_{0\le k\le K-1}$. Among others, a possible approach consists in adopting vectors $\boldsymbol{\lambda}_k(\boldsymbol{r})$ that recursively rotate the null-space basis such that the orthonormal waveforms are independent of the local null-space basis, hence unique within the null space.

Notice that any waveform generated from (5) or (6) is rank-one spanning one DoF on a proper basis, regardless of the coefficient vector $\boldsymbol{\lambda}_k(\boldsymbol{r})$ considered. This idea is a cornerstone of the work as it provides maximum flexibility in the waveform

[2]Under the block frequency-flat fading assumption, note that $\boldsymbol{H}^{(q)}_{\mathrm{OI}}(\boldsymbol{r}) = h^{(q)}_{\mathrm{OI},l}(\boldsymbol{r})\boldsymbol{I}_N \in \mathbb{C}^{N\times N}$.

[3]The multiplicity of the null-space eigenvalues is larger than one with high probability, and thus the null space bases provided by the associated eigenvectors are not unique implying that the designed waveforms are not unique either.

Table I: Particular notation used throughout this paper.

$\boldsymbol{r}_{\mathrm{T}}$, $\boldsymbol{r}_{\mathrm{R}}$	Positioning coordinates of the inner transmitter (T) and the inner receiver (R)
$h_{\mathrm{II},l}$	Inner channel coefficient for the block frequency-flat fading model
$h_{\mathrm{OI},l}^{(q)}(\boldsymbol{r})$	Interference-channel coefficient at position $\boldsymbol{r}$ for the block frequency-flat fading model
$\widehat{\boldsymbol{U}}_{\mathcal{N}}(\boldsymbol{r}) \in \mathbb{C}^{N\times M(\boldsymbol{r})}$	Null-space basis sensed at the inner node located at position $\boldsymbol{r}$
$\widetilde{\boldsymbol{U}}_{\mathcal{N}}(\boldsymbol{r}) \in \mathbb{C}^{N\times (M(\boldsymbol{r})-N_E(\boldsymbol{r}))}$	Basis of the correctly sensed available DoF at the inner node located at position $\boldsymbol{r}$
$\boldsymbol{E}_{\mathcal{N}}(\boldsymbol{r}) \in \mathbb{C}^{N\times N_E(\boldsymbol{r})}$	Null-space sensing error matrix at the inner node located at position $\boldsymbol{r}$
$M(\boldsymbol{r})$	Number of DoF sensed as available at the inner node located at position $\boldsymbol{r}$
$N_E(\boldsymbol{r})$	No. of occupied DoF wrongly sensed as available at the inner node located at position $\boldsymbol{r}$
$\boldsymbol{\lambda}_k(\boldsymbol{r}) \in \mathbb{C}^{M(\boldsymbol{r})}$	k-th coefficient vector at the inner node located at position $\boldsymbol{r}$
$\boldsymbol{\phi}_k = \widehat{\boldsymbol{U}}_{\mathcal{N}}(\boldsymbol{r}_{\mathrm{T}})\boldsymbol{\lambda}_k(\boldsymbol{r}_{\mathrm{T}}) \in \mathbb{C}^N$	k-th shaping transmission waveform
$\boldsymbol{\psi}_k = \widehat{\boldsymbol{U}}_{\mathcal{N}}(\boldsymbol{r}_{\mathrm{R}})\boldsymbol{\lambda}_k(\boldsymbol{r}_{\mathrm{R}}) \in \mathbb{C}^N$	k-th matched-filter receiving waveform

shaping design.

Regarding (5)–(6), identifying the null-space basis $\widehat{\boldsymbol{U}}_{\mathcal{N}}(\boldsymbol{r})$ is a critical aspect. A regular criterion without a priori information on the outer networks consists of a model order selection on the eigenvectors' matrix of the observations' autocorrelation matrix $\boldsymbol{R}_{\boldsymbol{xx}}(\boldsymbol{r}) = \boldsymbol{U}(\boldsymbol{r})\boldsymbol{\Lambda}(\boldsymbol{r})\boldsymbol{U}^H(\boldsymbol{r})$, where $\boldsymbol{U}(\boldsymbol{r}) \in \mathbb{C}^{N\times N}$ is the autocorrelation's eigenmatrix[4] and $\boldsymbol{\Lambda}(\boldsymbol{r}) \in \mathbb{C}^{N\times N}$ is a diagonal matrix containing the autocorrelation's eigenvalues sorted in non-increasing order.

From the autocorrelation decomposition, a critical partitioning of the eigenmatrix is $\boldsymbol{U}(\boldsymbol{r}) = \left[\begin{array}{c:c} \widehat{\boldsymbol{U}}_{\mathcal{S}}(\boldsymbol{r}) & \widehat{\boldsymbol{U}}_{\mathcal{N}}(\boldsymbol{r}) \end{array}\right]$, where $\widehat{\boldsymbol{U}}_{\mathcal{S}}(\boldsymbol{r}) \in \mathbb{C}^{N\times (N-M(\boldsymbol{r}))}$ spans the sensed occupied dimensions or DoF, and $\widehat{\boldsymbol{U}}_{\mathcal{N}}(\boldsymbol{r})$ spans the considered available DoF and from now on formally known as *null space*.

C. Mathematical Problem Formulation

In practice, the partition of $\boldsymbol{U}(\boldsymbol{r})$ suffers from several uncertainties: false-alarm and miss-detection errors, which depend on the estimation of $\boldsymbol{R}_{\boldsymbol{xx}}(\boldsymbol{r})$ and the subspace thresholding, that is, the criterion that determines which network resources are available or occupied, the time-varying nature of the wireless environment, and the sensing conditions at each location $\boldsymbol{r}$, among others. The combination of these uncertainties yields the *subspace leakage* problem [34], that is, the occupied network resources wrongly included in the opportunistic-operating null space; thus a more realistic model for the null-space basis $\widehat{\boldsymbol{U}}_{\mathcal{N}}(\boldsymbol{r})$ is given by

$$\widehat{\boldsymbol{U}}_{\mathcal{N}}(\boldsymbol{r}) = \left[\begin{array}{c:c} \widetilde{\boldsymbol{U}}_{\mathcal{N}}(\boldsymbol{r}) & \boldsymbol{E}_{\mathcal{N}}(\boldsymbol{r}) \end{array}\right], \tag{8}$$

where $\widetilde{\boldsymbol{U}}_{\mathcal{N}}(\boldsymbol{r}) \in \mathbb{C}^{N\times (M(\boldsymbol{r})-N_E(\boldsymbol{r}))}$ encompasses the correctly sensed available DoF, whereas $\boldsymbol{E}_{\mathcal{N}}(\boldsymbol{r}) \in \mathbb{C}^{N\times N_E(\boldsymbol{r})}$ models the sensing errors containing the critical $N_E(\boldsymbol{r})$ occupied DoF wrongly sensed as available. Hence, the orthonormal waveforms defined in (5)–(6) read as

$$\boldsymbol{\phi}_k = \widehat{\boldsymbol{U}}_{\mathcal{N}}(\boldsymbol{r}_{\mathrm{T}})\boldsymbol{\lambda}_k(\boldsymbol{r}_{\mathrm{T}}) = \left[\begin{array}{c:c} \widetilde{\boldsymbol{U}}_{\mathcal{N}}(\boldsymbol{r}_{\mathrm{T}}) & \boldsymbol{E}_{\mathcal{N}}(\boldsymbol{r}_{\mathrm{T}}) \end{array}\right] \boldsymbol{\lambda}_k(\boldsymbol{r}_{\mathrm{T}}). \tag{9}$$

$$\boldsymbol{\psi}_k = \widehat{\boldsymbol{U}}_{\mathcal{N}}(\boldsymbol{r}_{\mathrm{R}})\boldsymbol{\lambda}_k(\boldsymbol{r}_{\mathrm{R}}) = \left[\begin{array}{c:c} \widetilde{\boldsymbol{U}}_{\mathcal{N}}(\boldsymbol{r}_{\mathrm{R}}) & \boldsymbol{E}_{\mathcal{N}}(\boldsymbol{r}_{\mathrm{R}}) \end{array}\right] \boldsymbol{\lambda}_k(\boldsymbol{r}_{\mathrm{R}}). \tag{10}$$

The conventional null-space solution (7) is not robust to the subspace leakage errors encompassed in $\boldsymbol{E}_{\mathcal{N}}(\boldsymbol{r})$, which can lead to severe inter-system interferences that corrupt the outer-network communications. From (1) and (9)–(10), the impact of the sensing errors $\boldsymbol{E}_{\mathcal{N}}(\boldsymbol{r})$ in terms of the average total inter-system interference power is measured as

$$I_T(\boldsymbol{E}_{\mathcal{N}}(\boldsymbol{r}); \boldsymbol{\lambda}_k(\boldsymbol{r})) = \frac{1}{N}\sum_{k=0}^{K-1} \left\| \boldsymbol{E}_{\mathcal{N}}^H(\boldsymbol{r})\widehat{\boldsymbol{U}}_{\mathcal{N}}(\boldsymbol{r})\boldsymbol{\lambda}_k(\boldsymbol{r}) \right\|^2. \tag{11}$$

Note that (11) measures the interference level at the inner transmitter output or at the inner receiver input, without taking into account that the unknown path losses decrease both the interference imposed on each outer-network receiver by the inner transmitter and the interference leaked on the inner receiver by each outer-network transmitter. Although (11) seems a pessimistic metric, it is the best that can be done when the inner nodes do not have any a priori information about the outer networks, including their topology, the number of involved transmitter-receiver pairs, or the coded-modulation schemes, and the interference-channel coefficients are unknown.

We can now state that the objective of this work consists in designing $\{\boldsymbol{\lambda}_k(\boldsymbol{r})\}_{0\le k\le K-1}$ that minimizes the worst-case inter-system interferences, that is

$$\{\boldsymbol{\lambda}_k(\boldsymbol{r})\}_{0\le k\le K-1} = \underset{\{\boldsymbol{\lambda}_k(\boldsymbol{r})\}}{\arg\min} \max_{\boldsymbol{E}_{\mathcal{N}}(\boldsymbol{r})} I_T(\boldsymbol{E}_{\mathcal{N}}(\boldsymbol{r}); \boldsymbol{\lambda}_k(\boldsymbol{r})) \tag{12a}$$

$$\text{subject to} \quad \|\boldsymbol{E}_{\mathcal{N}}(\boldsymbol{r})\|_{\mathrm{F}}^2 \le \xi^2 \tag{12b}$$

$$\boldsymbol{\lambda}_k^H(\boldsymbol{r})\boldsymbol{\lambda}_{k'}(\boldsymbol{r}) = 0,\ k \ne k' \tag{12c}$$

$$\boldsymbol{\lambda}_k^H(\boldsymbol{r})\widehat{\boldsymbol{U}}_{\mathcal{N}}^H(\boldsymbol{r})\boldsymbol{e}_k = \alpha_k \tag{12d}$$

[4]This is not the unique criterion. Instead of using the eigenmatrix, any arbitrary orthonormal matrix $\boldsymbol{U}(\boldsymbol{r}) \in \mathbb{C}^{N\times N}$ obtained using any additional information on the outer networks is a valid DoF basis. In some cases, a pseudo-random basis could be interesting to break any systematic error and further decrease the residual interferences. We show in Section III that the designed waveforms is independent of the considered subspace basis, and hence any related discussion is out of the scope of this work.

Note that some constraints are required to avoid the min-max design problem in (12a) to being ill-posed. In particular, (12b) upper-bounds the degree of uncertainty assumed in the sensing error model in (9)–(10), being $\xi^2 \in \mathbb{R}^+$; (12c) guarantees the orthogonality between the designed waveforms $\{\boldsymbol{\phi}_k\}_{0\leq k\leq K-1}$ or $\{\boldsymbol{\psi}_k\}_{0\leq k\leq K-1}$; and (12d) is a non-trivial design constraint, with

$$\boldsymbol{e}_k \triangleq \left[\mathbf{0}_{n(k)-1}^T \; 1 \; \mathbf{0}_{N-n(k)}^T\right]^T, \;\; n(k) \in \{1,\ldots,N\}, \quad (13)$$

an N-length selection vector and $\alpha_k \in \mathbb{R}^+$ such that $\|\boldsymbol{\phi}_k\|^2 = 1$. The constraint (12d) not only avoids a trivial all-zeros solution but it also implies the introduction of a classical linear prediction-based solution as shown in [37]. In many problems, the selection of the subindex $n(k)$ is arbitrary, but for the problem at hand, the paper shows in Section III that it can be optimized to provide minimum residual inter-system interference (11).

Recalling the constraint (12b), it is interesting to note that, as $\boldsymbol{E}_{\mathcal{N}}(\boldsymbol{r})$ is left-unitary, then $\|\boldsymbol{E}_{\mathcal{N}}(\boldsymbol{r})\|_{\mathrm{F}}^2 = \mathrm{tr}[\boldsymbol{E}_{\mathcal{N}}^H(\boldsymbol{r})\boldsymbol{E}_{\mathcal{N}}(\boldsymbol{r})] = \mathrm{rank}[\boldsymbol{E}_{\mathcal{N}}(\boldsymbol{r})] \leq \xi^2$. Thus, this constraint only affects the maximum number of assumed erroneous null-space dimensions or DoF, which is the most restrictive constraint for the unstructured error model in (8) (cf. [38] and references therein).

As a final comment, note that the problem formulated in (12a)–(12d) is equivalent to a Minimum-Norm Total Least-Squares (MNTLS) optimization problem [39]–[41], which is of paramount interest in many engineering disciplines. It is well-known that the solution to the MNTLS problem exhibits robustness to data modeling errors and is unique within the vector space it lies in. The former reveals the optimality of the designed waveforms under worst-case interferences, whereas the latter provides the waveforms with a self-calibration property. As discussed in Section III-B, the self-calibration property is fundamental to drastically reducing the feedback overheads.

III. General Solution

In this section, we describe the solution to the waveform design problem in (12a), and we provide its main properties. As the objective function is the same at both inner nodes, we first focus on the inner transmitting node without loss of generality. Accordingly, the positioning coordinates $\boldsymbol{r}_{\mathrm{T}}$ are omitted when possible for notational simplicity. Then, the interference mitigation capability of the proposed waveforms is studied in Section III-A, whereas the properties of the derived waveforms as receiving filters are studied in Section III-B.

The design of the class of linear modulations $\{\boldsymbol{\phi}_k\}_{0\leq k\leq K-1}$ defined in (9) and satisfying (12a)–(12d) is summarized in the following proposition.

Proposition 1. *The $\{\boldsymbol{\phi}_k\}_{0\leq k\leq K-1}$ satisfying* (12a)–(12d) *is based on the orthogonal projector onto the null space $\left\langle \widehat{\boldsymbol{U}}_{\mathcal{N}} \right\rangle$, given by $\widehat{\boldsymbol{P}}_0 = \widehat{\boldsymbol{U}}_{\mathcal{N}}\widehat{\boldsymbol{U}}_{\mathcal{N}}^H \in \mathbb{C}^{N\times N}$. So as to guarantee the orthogonality between the K waveforms, a sequential dimensionality reduction of the null space is required such that $\widehat{\boldsymbol{P}}_{k+1} = \widehat{\boldsymbol{P}}_k\left(\boldsymbol{I}_N - \boldsymbol{\phi}_k\boldsymbol{\phi}_k^H\right)$. Therefore, each pulse-shaping waveform $\boldsymbol{\phi}_k$ is given by*

$$\boldsymbol{\phi}_k = \gamma_k \widehat{\boldsymbol{P}}_k \boldsymbol{e}_k, \text{ for } k = 0\ldots, K-1, \quad (14)$$

where $\gamma_k = (\boldsymbol{e}_k^T\widehat{\boldsymbol{P}}_k\boldsymbol{e}_k)^{-1/2}$ is a scaling factor that guarantees unit norm.

Proof: See Appendix A. ∎

Algorithm 1 Sequential Design of $\{\boldsymbol{\phi}_k\}_{0\leq k\leq K-1}$

Input: K, $\widehat{\boldsymbol{U}}_{\mathcal{N}}$
Output: $\{\boldsymbol{\phi}_k\}_{0\leq k\leq K-1}$
1: $\widehat{\boldsymbol{P}}_0 = \widehat{\boldsymbol{U}}_{\mathcal{N}}\widehat{\boldsymbol{U}}_{\mathcal{N}}^H$
2: **for** $k = 0$ until $K-1$ **do**
3: Find $\boldsymbol{e}_k = \left[\mathbf{0}_{n(k)-1}^T \; 1 \; \mathbf{0}_{N-n(k)}^T\right]^T$ using (15)
4: $\boldsymbol{\phi}_k = \gamma_k\widehat{\boldsymbol{P}}_k\boldsymbol{e}_k$ with $\gamma_k = (\boldsymbol{e}_k^T\widehat{\boldsymbol{P}}_k\boldsymbol{e}_k)^{-1/2}$
5: $\widehat{\boldsymbol{P}}_{k+1} = \widehat{\boldsymbol{P}}_k\left(\boldsymbol{I}_N - \boldsymbol{\phi}_k\boldsymbol{\phi}_k^H\right)$
6: **end for**

Recalling (13), it is worth noting that the k-th waveform $\boldsymbol{\phi}_k$ (14) is a certain scaled column of the corresponding projector $\widehat{\boldsymbol{P}}_k$. Appendix A also unveils that finding the orthogonal waveforms (14) inducing minimum worst-case inter-system interference involves designing (13) so as to select the column of $\widehat{\boldsymbol{P}}_k$ containing the largest main diagonal element. Nevertheless, in some situations, the main diagonal of $\widehat{\boldsymbol{P}}_k$ can be constant. To avoid coordination and design complexity, a sequential column selection can be adopted. Thus, the selection vector $\boldsymbol{e}_k$ can be designed as

$$n(k) = \begin{cases} k+1 & \text{if } \left[\widehat{\boldsymbol{P}}_k\right]_{nn} = C, \; 1\leq n\leq N \\ \underset{n\in\{1,\ldots,N\}}{\arg\max} \left[\widehat{\boldsymbol{P}}_k\right]_{nn} & \text{otherwise} \end{cases}, \quad (15)$$

where $k = 0\ldots, K-1$, $\left[\widehat{\boldsymbol{P}}_k\right]_{nn}$ is the n-th diagonal element of $\widehat{\boldsymbol{P}}_k$, and $C \in \mathbb{C}$ is a constant. Taking into account the abovementioned exposition, the whole set of K waveforms, henceforth denoted as Minimum-Norm Waveforms (MNWs), can be recursively found as in Algorithm 1.

At this point, we can compare the classic null-space approach in (7) with the solution in (14). As studied in detail in Appendix A, the linear combination coefficients vectors $\{\boldsymbol{\lambda}_k\}_{0\leq k\leq K-1}$ solving (12a)–(12d) can be written as

$$\boldsymbol{\lambda}_k = \gamma_k\widehat{\boldsymbol{U}}_{\mathcal{N}}^H\left[\boldsymbol{I}_N - \sum_{k'=0}^{k-1}\boldsymbol{\phi}_{k'}\boldsymbol{\phi}_{k'}^H\right]\boldsymbol{e}_k = \boldsymbol{M}_k\boldsymbol{e}_k, \quad (16)$$

for $k = 0,\ldots,K-1$, where the selection vector $\boldsymbol{e}_k$ is given in (13) and $\boldsymbol{M}_k$ is a transformation matrix. In view of (16), note that both approaches (7) and (16) are based on a column selection on two different matrices. The classic approach in (7) makes use of an arbitrary column selection from the null-space $\widehat{\boldsymbol{U}}_{\mathcal{N}}$ matrix, without taking into account any optimization criterion. Instead, the MNTLS approach in (16) implies the use of a waveform obtained by selecting a column from the projection matrix of the sensed null space. The column selection is now performed in order to minimize

the induced interference due to sensing errors, that is, to the imperfect knowledge of the null space. Finally, it is also worth mentioning that the waveforms obtained from the projection matrix are all invariant to the originally adopted sensing reference basis $\widehat{\boldsymbol{U}}_{\mathcal{N}}$, which simplifies the coordination network overhead, as it will be discussed in Section III-B.

A. Technical Discussion

The former waveform design problem (12a)–(12d) admits an interpretation in terms of maximizing the achieved worst-case transmitted signal-to-interference ratio ($\mathrm{SIR_T}$). In this sense, the total average transmitted power is given by $S_T = \sum_{k=0}^{K-1} \|\boldsymbol{\phi}_k\|^2 / N = \sum_{k=0}^{K-1} \|\boldsymbol{\lambda}_k\|^2 / N$. This expression includes the orthogonal signal power plus the residual interference. The design criterion in (12a) becomes equivalent to the max-min criterion on the quotient $S_T/I_T = \mathrm{SIR_T}+1$, where the interference power I_T is defined in (11), and thus, the following proposition holds.

Proposition 2. *The objective function in* (12a) *is equivalent to*

$$\{\boldsymbol{\lambda}_k\}_{0\le k\le K-1} = \arg\max_{\{\boldsymbol{\lambda}_k\}} \min_{\boldsymbol{E}_{\mathcal{N}}} \mathrm{SIR_T}\left(\boldsymbol{E}_{\mathcal{N}}; \boldsymbol{\lambda}_k\right), \tag{17}$$

leading to an achievable $\mathrm{SIR_T}$ *given by*

$$\mathrm{SIR_T}(\boldsymbol{E}_{\mathcal{N}}; \boldsymbol{\lambda}_k) = \frac{K}{\sum_{k=0}^{K-1} \left(f_k\left(\widehat{\boldsymbol{P}}_{\mathcal{E}}\right) / \left[\widehat{\boldsymbol{P}}_k\right]_{nn}\right)} - 1, \tag{18}$$

where $f_k(\widehat{\boldsymbol{P}}_{\mathcal{E}})$ *is a positive function that depends on both the waveform index* k *and the unknown projector* $\widehat{\boldsymbol{P}}_{\mathcal{E}}$ *onto* $\langle \boldsymbol{E}_{\mathcal{N}} \rangle$.

Proof: See Appendix B. ∎

Hence, the design approach in (12a)–(12d) provides the waveform with the maximum worst-case $\mathrm{SIR_T}$, which is the best that can be done under feedforward conditions. Note that the optimum receiver approach maximizing the signal-to-interference-plus-noise ratio (SINR) cannot be considered in feedforward settings due to the lack of coordination between the inner transmitter and receiver.

Regarding the achievable $\mathrm{SIR_T}$ (18), it is not possible to know the operating $\mathrm{SIR_T}$, as the denominator in (18) depends on the unknown error matrix $\boldsymbol{E}_{\mathcal{N}}$. However, (18) reveals that achieving the maximum $\mathrm{SIR_T}$ requires finding the largest diagonal element of the matrix $\widehat{\boldsymbol{P}}_k$, pointing up the importance of the minimum-norm design condition in (15).

Notice that (18) accounts for the aggregate interference induced on all erroneous null-space dimensions, which is very pessimistic in terms of measuring the impact on the outer receivers. A more appropriate performance metric should measure the ratio between the opportunistic orthogonal signal power and the interference induced per erroneous dimension. Consequently, we define the so-called Signal-to-Interference Density Ratio ($\mathrm{SIDR_T}$) at the transmitter output as

$$\mathrm{SIDR_T} \triangleq \frac{S_T - I_T}{I_T / N_E} \tag{19}$$

where $N_E = \mathrm{rank}[\boldsymbol{E}_{\mathcal{N}}]$ is the number of wrongly sensed available DoF. Although $\mathrm{SIDR_T}$ does not admit a closed-form expression for finite N, a simple asymptotic characterization is stated in the following proposition.

Proposition 3. *For large enough* N, $\mathrm{SIDR_T}$ *admits a simple analytical expression given by*

$$\mathrm{SIDR_T}(\boldsymbol{E}_{\mathcal{N}}; \boldsymbol{\lambda}_k) \approx N \cdot \frac{M}{N} \cdot \left(1 - \frac{N_E}{M}\right). \tag{20}$$

Proof: See Appendix C. ∎

Note that (20) is based on the number of total DoF N; the level of the *sensed* DoF availability M/N, with $M = \mathrm{rank}[\widehat{\boldsymbol{U}}_{\mathcal{N}}]$; and the *inaccuracy* of the null-space sensing scheme N_E/M, which accounts for the impact of sensing uncertainties described in Section II-C.

The tightness of the approximation given in (20) is numerically validated in Figure 2, where the $\mathrm{SIDR_T}$ is depicted as a function of the *sensed* DoF availability M/N, for different N and different relative sensing errors N_E/M. We numerically verified that $\mathrm{SIDR_T}$ is independent of K, as reflected in (20), being the conclusions valid for all $K \le M$. We observe that the sensing errors are critical at low M/N. However, when the system bandwidth is reasonably large (large N), the MNWs exhibit outstanding performance in terms of $\mathrm{SIDR_T}$. The robustness of the proposed solution to undesired inter-system interferences is illustrated in Figure 3, where we note that an unrealistic N_E/M is necessary to heavily decrease the $\mathrm{SIDR_T}$ performance.

The robustness to inter-system interferences exhibited by the MNWs can also be understood from the DoF-based signal spreading capability of (14) stated in the following proposition.

Proposition 4. *Any solution* $\boldsymbol{\phi}_k$ *from* (14) *spreads or distributes the transmitted power or energy along all the available sensed null-space dimensions, and it asymptotically performs a uniform allocation when the number of total dimensions* N *is arbitrarily large.*

Proof: See Appendix D. ∎

This property implies that the residual inter-system interference power is maximally spread over the whole available sensed DoF, breaking the structure of residual interferences and minimizing the interference density per DoF. Nonetheless, this spreading does not imply that one single MNW saturates the sensed null space. Recalling Algorithm 1, it is possible to find orthogonal waveforms that span one DoF per waveform on a self-calibrated null-space basis.

B. Invariance and Receiving Scheme

One of the main properties of the designed transmission scheme is that the MNWs are obtained by selecting certain columns of a projection matrix and, thus, being independent of the null-space basis at each inner node. Therefore, if and only if the null spaces sensed at each inner node are equal, the following proposition holds.

Proposition 5. *Let* $\widehat{\boldsymbol{U}}_{\mathcal{N}}(\boldsymbol{r}_T) \in \mathbb{C}^{N\times M(\boldsymbol{r}_T)}$ *and* $\widehat{\boldsymbol{U}}_{\mathcal{N}}(\boldsymbol{r}_R) \in \mathbb{C}^{N\times M(\boldsymbol{r}_R)}$ *be the sensed null-space bases at the inner transmitter and receiver, respectively. If* $\left\langle \widehat{\boldsymbol{U}}_{\mathcal{N}}(\boldsymbol{r}_T) \right\rangle = \left\langle \widehat{\boldsymbol{U}}_{\mathcal{N}}(\boldsymbol{r}_R) \right\rangle$,

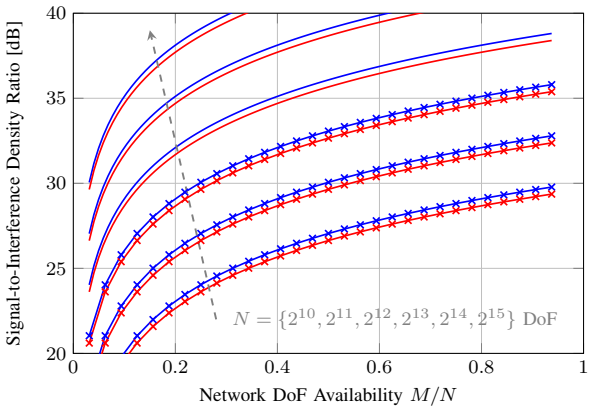

Fig. 2: Simulated $\mathrm{SIDR}_{\mathrm{T}}$ (marks) and the theoretical model in (20) (lines) vs. the network DoF availability M/N, for different N and with $N_E/M = 0.01$ (blue) and $N_E/M = 0.1$ (red).

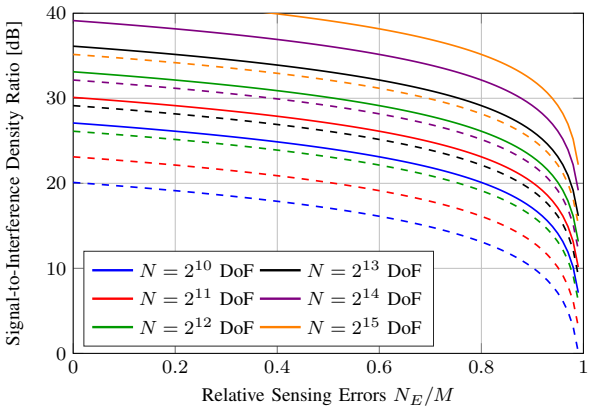

Fig. 3: Theoretical model for the $\mathrm{SIDR}_{\mathrm{T}}$ (20) vs. the null-space sensing inaccuracy N_E/M, for different N and with $M/N = 0.1$ (dashed) and $M/N = 0.5$ (solid).

and thus, $M(\boldsymbol{r}_T) = M(\boldsymbol{r}_R) = M$, the k-th transmitting waveform $\boldsymbol{\phi}_k$ and the k-th receiving waveform $\boldsymbol{\psi}_k$ are equal.

Proof: If $\left\langle \widehat{\boldsymbol{U}}_{\mathcal{N}}(\boldsymbol{r}_{\mathrm{T}}) \right\rangle = \left\langle \widehat{\boldsymbol{U}}_{\mathcal{N}}(\boldsymbol{r}_{\mathrm{R}}) \right\rangle$, that is, the inner transmitting and receiving node sense the same null space, there exist an $M \times M$ right-unitary matrix $\boldsymbol{Q}$ such that $\widehat{\boldsymbol{U}}_{\mathcal{N}}(\boldsymbol{r}_{\mathrm{T}}) = \widehat{\boldsymbol{U}}_{\mathcal{N}}(\boldsymbol{r}_{\mathrm{R}})\boldsymbol{Q}$. Thus, $\widehat{\boldsymbol{P}}_{0,\mathrm{T}} = \widehat{\boldsymbol{U}}_{\mathcal{N}}(\boldsymbol{r}_{\mathrm{T}})\widehat{\boldsymbol{U}}_{\mathcal{N}}^H(\boldsymbol{r}_{\mathrm{T}}) = \widehat{\boldsymbol{U}}_{\mathcal{N}}(\boldsymbol{r}_{\mathrm{R}})\boldsymbol{Q}\boldsymbol{Q}^H\widehat{\boldsymbol{U}}_{\mathcal{N}}^H(\boldsymbol{r}_{\mathrm{R}}) = \widehat{\boldsymbol{P}}_{0,\mathrm{R}}$, and, therefore, Algorithm 1 provides the same waveforms regardless of the input sensed null-space basis. ■

In accordance with Proposition 5, the MNWs are independent of the considered subspace basis and, thus, invariant within the orthogonal subspace. The major consequence of the invariance property is that the minimum worst-case interference design criterion described in Section II-C provides a matched-filter receiver with interference cancellation capabilities that is self-calibrated with the inner transmitter despite the lack of interaction between inner nodes. In contrast to classic null-space approaches (7), where Proposition 5 does not hold, the feedback overheads required to calibrate the opportunistic transmission and reception null spaces can be avoided.

Nevertheless, in practice, the null spaces at inner transmitter and receiver nodes differ, that is $\left\langle \widehat{\boldsymbol{U}}_{\mathcal{N}}(\boldsymbol{r}_{\mathrm{T}}) \right\rangle \neq \left\langle \widehat{\boldsymbol{U}}_{\mathcal{N}}(\boldsymbol{r}_{\mathrm{R}}) \right\rangle$. This *subspace mismatch* is the consequence of basing the distributed waveform design on local-only null-space sensing, without cooperation between inner nodes.

At this point, we shall discuss the impact of this subspace mismatch on opportunistic communication performance. The subspace mismatch incurs two major performance losses on the inner receiver. On the one hand, since the inner transmitter may use some DoF that do not belong to the inner-receiver null space, a fraction of the transmitted energy is lost. In this sense, we study the detection relative energy loss ratio, i.e.,

$$\Gamma_K \triangleq \frac{\sum_{k=0}^{K-1} \|\boldsymbol{\phi}_k\|^2}{\sum_{k=0}^{K-1} \|\boldsymbol{\psi}_k^H \boldsymbol{\phi}_k\|^2}. \tag{21}$$

Note that the numerator is the transmitted energy and the denominator measures the received energy after matched filtering. On the other hand, since the orthogonal projectors are slightly different under subspace mismatch, the opportunistic communication also suffers from the loss of orthogonality between transmitted waveforms after matching filtering, that is, $\boldsymbol{\psi}_{k'}^H \boldsymbol{\phi}_k \neq 0$, for $k \neq k'$, incurring inter-symbol interference (ISI). This aspect is analyzed through the ISI to signal energy ratio given by

$$\mathrm{ISR}_{\mathrm{sm}}[K] \triangleq \frac{\sum_{k=0}^{K-1} \sum_{k'=0, k' \neq k}^{K-1} \|\boldsymbol{\psi}_{k'}^H \boldsymbol{\phi}_k\|^2}{\sum_{k=0}^{K-1} \|\boldsymbol{\psi}_k^H \boldsymbol{\phi}_k\|^2}, \tag{22}$$

where the numerator measures the loss of orthogonality between transmitted waveforms and matched filters. Note that the numerator is zero when $\left\langle \widehat{\boldsymbol{U}}_{\mathcal{N}}(\boldsymbol{r}_{\mathrm{T}}) \right\rangle = \left\langle \widehat{\boldsymbol{U}}_{\mathcal{N}}(\boldsymbol{r}_{\mathrm{R}}) \right\rangle$.

In general, the analysis of both (21) and (22) are highly involved and numerical performance evaluation is required. If we focus on (21), and in order to circumvent the recursive nature of (14), we may notice that the design conditions do not largely change at the different recursive stages. Thus, the absolute total detected energy loss can be reasonably approximated by K times the loss on a single waveform. This is why $K = 1$ can be of major interest, as it can provide the simple tight approximation to the addressed problem given in the following proposition.

Proposition 6. *For $K = 1$ and large enough N, (21) is given by*

$$\Gamma_1 = \frac{\boldsymbol{\phi}_0^H \boldsymbol{\phi}_0}{|\boldsymbol{\psi}_0^H \boldsymbol{\phi}_0|^2} \xrightarrow[N \to +\infty]{} 1 + \rho_T + \rho_R + \rho_T \rho_R, \tag{23}$$

where $\rho_T \triangleq \kappa_T / M_0$ and $\rho_R \triangleq \kappa_R / M_0$ denote the normalized uncertainties at inner transmitter and receiver, respectively; being M_0 the dimension of the active null space $\mathcal{N}_0 = \langle \widehat{\boldsymbol{U}}_{\mathcal{N}}(\boldsymbol{r}_T) \rangle \cap \langle \widehat{\boldsymbol{U}}_{\mathcal{N}}(\boldsymbol{r}_R) \rangle$, and κ_T and κ_R the DoF excess at the inner transmitter and receiver.

Proof: See Appendix E. ■

The behavior predicted by (23) is compared with numerical simulations in Figure 4. We see that (23) reliably approximates the energy loss, especially for small K. We also observe that Γ_K is smaller than 0.5 dB for $\rho_{\mathrm{T}} \leq 0.1$, that is, the DoF excess at the inner transmitter is the 10% of M_0. This numerical result validates the theoretical analysis in Appendix E and the former assumption that the relative energy detection loss in

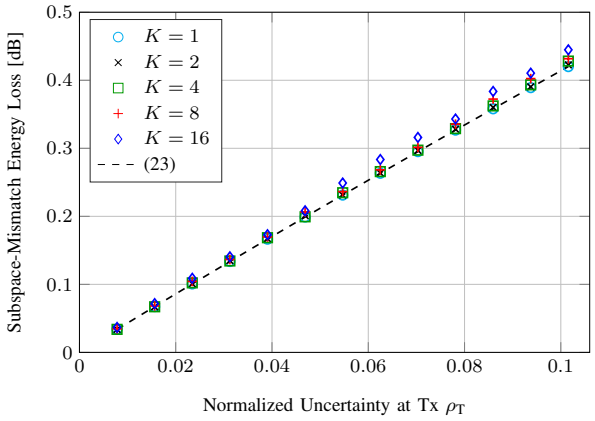

Fig. 4: Γ_K (21) in dB vs. ρ_{T}, with $N = 1024$, $M_0 = N/8$ and $\rho_{\mathrm{R}} = 0$, for different K.

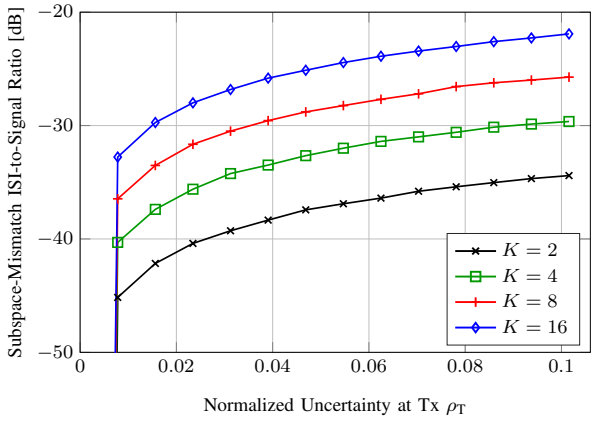

Fig. 5: $\mathrm{ISR}_{\mathrm{sm}}[K]$ (22) in dB vs. ρ_{T}, with $N = 1024$, $M_0 = N/8$, and $\rho_{\mathrm{R}} = 0$, for different K.

(21) is almost constant with K.

Regarding the loss of orthogonality of the transmitted waveforms, the recursive nature of the algorithm cannot be unfortunately circumvented. Thus, analytical characterization of (22) has not been found. Figure 5 numerically evaluates the degree of robustness of the proposed communication scheme to subspace mismatch, and it shows that, under mild operating conditions, it is not critical for practical values of K.

In both Figures 4 and 5, we consider the case $\rho_{\mathrm{R}} = 0$. Note that the inner receiver can locally improve its performance using an active subspace detection scheme, as in [42]. Unlike classic null-space solutions (7), which need to agree on a common null-space transmitting and receiving basis for coherent opportunistic communication, the inner receiver only needs to identify $\mathcal{N}_0$ regardless of the considered null-space basis thanks to the discussed invariance property.

IV. Asymptotic Behavior and Efficient Implementations

This section characterizes the behavior of the MNWs (14) when the total number of DoF is arbitrarily large. We will see that, under asymptotic conditions, the design complexity will depend on the complexity of the scenario. In particular, for the specific case discussed in Section IV-A, the MNWs exhibit a circulant behavior defining a cyclic time-multiplexing scheme. Finally, Section IV-B discusses the adaptation of the communication scheme derived in this work to frequency-selective channels.

A well-known general result [43] is that any $N \times N$ autocorrelation matrix admits an asymptotic spectral factorization given by $\boldsymbol{F}^H \boldsymbol{\Lambda}_F \boldsymbol{F}$, where $\boldsymbol{F} \in \mathbb{C}^{N\times N}$ is the unitary Fourier matrix and $\boldsymbol{\Lambda}_F \in \mathbb{C}^{N\times N}$ is the diagonal matrix with elements equal to the power spectral density distribution. Thus, the null-space basis $\widehat{\boldsymbol{U}}_{\mathcal{N}}(\boldsymbol{r})$ will asymptotically be composed of a subset of column vectors of $\boldsymbol{F}^H$. In this sense, we define the set of indices of available DoF (asymptotically, frequency bins) as $\mathcal{I}_{\mathcal{N}}(\boldsymbol{r}) \triangleq \left\{m \;:\; \boldsymbol{f}_m \in \left\langle \widehat{\boldsymbol{U}}_{\mathcal{N}}(\boldsymbol{r}) \right\rangle \right\}$, where $\boldsymbol{f}_m \in \mathbb{C}^N$ is the m-th column of $\boldsymbol{F}^H$.

Under these conditions, the MNWs asymptotically behave as in the following proposition.

Proposition 7. *The MNWs satisfying* (14) *asymptotically rely on the circulant orthogonal projector* $\widehat{\boldsymbol{P}}_0(\boldsymbol{r}) = \sum_{m\in\mathcal{I}_{\mathcal{N}}(\boldsymbol{r})} \boldsymbol{f}_m \boldsymbol{f}_m^H$, *whose diagonal elements are constant and equal to* $M(\boldsymbol{r})/N$, *and thus are asymptotically based on linear combinations of complex exponentials.*

Proof: Based on (14)–(15), the first transmitting MNW $\boldsymbol{\phi}_0$ relies on the first column of $\widehat{\boldsymbol{P}}_0(\boldsymbol{r}_{\mathrm{T}})$, and thus the n-th element of $\boldsymbol{\phi}_0$ is given by

$$\phi_0[n] = \frac{1}{\sqrt{M(\boldsymbol{r}_{\mathrm{T}})N}} \sum_{\forall m\in\mathcal{I}_{\mathcal{N}}(\boldsymbol{r}_{\mathrm{T}})} e^{j\frac{2\pi}{N}nm}, \tag{24}$$

for $n = 0, \ldots, N-1$, where $M(\boldsymbol{r}_{\mathrm{T}}) = \mathrm{rank}\left[\widehat{\boldsymbol{U}}_{\mathcal{N}}(\boldsymbol{r}_{\mathrm{T}})\right]$. Note that (24) can be vectorized and decomposed as

$$\boldsymbol{\phi}_0 = \gamma_0 \boldsymbol{f}_{m_{\min}} \odot \sum_{\forall m\in\mathcal{I}_{\mathcal{N}}(\boldsymbol{r}_{\mathrm{T}})} \boldsymbol{f}_{m-m_{\min}}, \tag{25}$$

being γ_0 a scaling factor that guarantees unit norm, the index $m_{\min}$ is given by $m_{\min} = \min\{m \;:\; m \in \mathcal{I}_{\mathcal{N}}(\boldsymbol{r}_{\mathrm{T}})\}$ and $[\boldsymbol{f}_{m-m_{\min}}]_n = N^{-1/2}\exp(j2\pi(m-m_{\min})n/N)$ for $n = 0, \ldots, N-1$. The remaining $K-1$ MNWs are derived from Algorithm 1 but cannot be expressed compactly as (25). ■

Although the proof of Proposition 7 is focused on the inner transmitter, note that it also holds at the inner receiver since the waveform design at both nodes is based on Algorithm 1.

In the sequel, we study the asymptotic behavior of the MNWs when the available sensed frequency bins are consecutive and the adaptation of the MNWs in frequency-selective channels.

A. Particular Case: Circulant-Shaping Time-Division Multiple Access (CS-TDMA)

This subsection studies the behavior of the general asymptotic solution in (24) for the particular case of consecutive available frequency bins, that is, $\mathcal{I}_{\mathcal{N}}(\boldsymbol{r}) = \{m_0, \ldots, m_0 + M(\boldsymbol{r}) - 1\}$, when the quotient $N/M(\boldsymbol{r})$ is an integer and/or asymptotically large.

Without loss of generality, the discussion will be focused on the transmitting waveform, and thus the dependence on the positioning vector $\boldsymbol{r}_{\mathrm{T}}$ will be omitted for simplicity. Under the

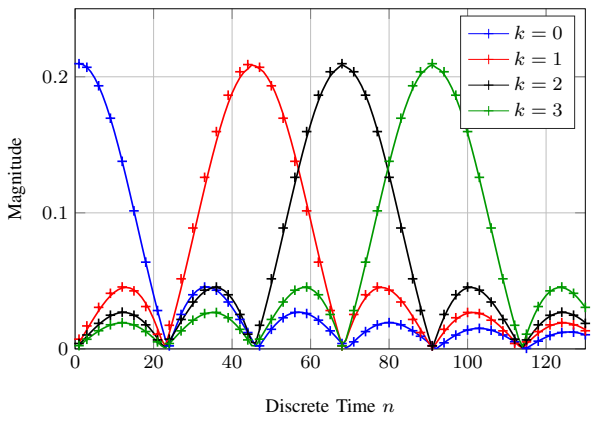

Fig. 6: Comparison of $\boldsymbol{\phi}_k$ (lines) designed according to the approximation with the corresponding scaled columns of $\widehat{\boldsymbol{P}}_0$ (marks), for $N = 1024$ and $M = 45$.

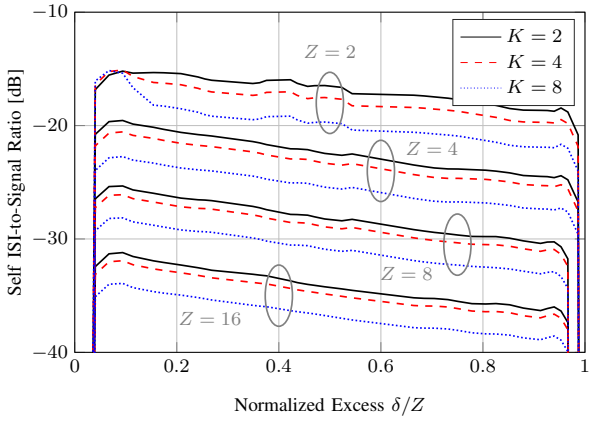

Fig. 7: Self Inter-Symbol Interference-to-Signal Ratio as a function of the relative excess δ/Z with $N = 1024$, for different integers Z and transmitted waveforms K.

conditions discussed above, (24) can be written as

$$\begin{aligned}\phi_0[n] &= \frac{1}{\sqrt{MN}} e^{j\frac{2\pi}{N}nm_0} \sum_{m=0}^{M-1} e^{j\frac{2\pi}{N}nm} \\ &= \frac{1}{\sqrt{MN}} \frac{\sin\left(M\frac{\pi n}{N}\right)}{\sin\left(\frac{\pi n}{N}\right)} e^{j\frac{\pi[(M-1)+2m_0]n}{N}}.\end{aligned} \tag{26}$$

According to Algorithm 1, the second MNW $\boldsymbol{\phi}_1$ is the appropriately scaled column of $\widehat{\boldsymbol{P}}_1 = \widehat{\boldsymbol{P}}_0 - \boldsymbol{\phi}_0\boldsymbol{\phi}_0^H$ containing the maximum diagonal element. Since the diagonal of $\widehat{\boldsymbol{P}}_0$ is constant in view of Proposition 7, $\boldsymbol{\phi}_1$ is found at the column n of $\widehat{\boldsymbol{P}}_1$ where

$$\phi_0[n]\phi_0^*[n] = \frac{1}{MN}\left(\frac{\sin\left(M\frac{\pi n}{N}\right)}{\sin\left(\frac{\pi n}{N}\right)}\right)^2 \tag{27}$$

is minimum. If N/M is an integer, note that (27) is 0 at $n = kN/M$, with k an integer. Moreover, noting that $\phi_0[n]\phi_0^*[kN/M] = 0$, for all possible k, it is straightforward to check that $\boldsymbol{\phi}_k$ is just the (kN/M)-th column of $\widehat{\boldsymbol{P}}_0$, for $k = 1, \ldots, K-1$. Taking into account the periodicity of the trigonometric functions, we have that $\phi_k\left[(n + kN/M) \bmod N\right] = \phi_0[n]$, for $n = 0, \ldots, N-1$, and therefore the remaining $K-1$ MNWs can be found as a permutation of $\boldsymbol{\phi}_0$, i.e.

$$\boldsymbol{\phi}_k = \boldsymbol{\Pi}_{\frac{kN}{M}}\boldsymbol{\phi}_0, \quad \text{for } k = 1, \ldots, K-1, \tag{28}$$

with $\boldsymbol{\Pi}_q = \left[\begin{array}{c:c} [\boldsymbol{I}_N]_{q+1:N} & [\boldsymbol{I}_N]_{1:q} \end{array}\right]$ an $N \times N$ permutation matrix, being $[\boldsymbol{I}_N]_{q:r}$ a subset of the identity matrix encompassing columns from q to r.

The particular interest in this solution is twofold. First, the whole set of K MNWs can be efficiently found, with no need of leveraging the sequential Algorithm 1. Note that the MNWs design becomes relatively simple in *structured* scenarios while requiring a sequential design as in Proposition 7 in more complex environments. Second, since the permutation practices a circular time-shift, (28) behaves similarly to time division multiple access (TDMA), employing specific signals. We will refer to this modulation as *Circulant-Shaping* TDMA (CS-TDMA).

In general, when the quotient N/M is not an integer, the remaining $K-1$ waveforms can be designed as follows: (i) design the first waveform $\boldsymbol{\phi}_0$ according to the MNTLS criterion, (ii) interpolate $\boldsymbol{\phi}_0$ to get an N'-length waveform $\tilde{\boldsymbol{\phi}}_0$ such that N'/M is an integer, (iii) find the $K-1$ remaining waveforms as in (28), and (iv) decimate the K waveforms to get N-size sequences.

This methodology leads to an approximation, whose performance is numerically evaluated in Figures 6 and 7. For ease of discussion, let $N/M = Z + \delta$, where Z is the whole number part and δ is the fractional part. In Figure 6, we compare the proposed approximation to the corresponding columns of $\widehat{\boldsymbol{P}}_0$ for the case $N/M = (900 + 124)/45 = 20 + 2.7556$, where $Z \gg \delta$. Even though the proposed efficient approximation reliably mimics the corresponding columns of $\widehat{\boldsymbol{P}}_0$, note that the waveforms do not have common zeros, leading to a self inter-symbol interference. The impact of this interference is assessed in Figure 7, where we depict the Self ISI-to-Signal Ratio, defined as $\left(\sum_{k=0}^{K-1}\sum_{k'=0,k'\neq k}^{K-1}\|\boldsymbol{\phi}_{k'}^H\boldsymbol{\phi}_k\|^2\right) / \left(\sum_{k=0}^{K-1}\|\boldsymbol{\phi}_k^H\boldsymbol{\phi}_k\|^2\right)$, as a function of the quotient δ/Z. The Self ISI becomes negligible when N/M can be approximated by an integer, which occurs when $\delta/Z \to 0$ and when $\delta/Z \to 1$. Note that these two cases hold in general when $M \ll N$, which corresponds to a congested network. The number of waveforms K plays the role of an SNR gain, and thus the useful signal becomes stronger than the interferences, which decreases the ratio illustrated in Figure 7. As a final remark, small values of the quotient N/M reveal that the network is not congested, and hence the inner nodes may virtually decrease M to obtain an integer quotient N/M. Nevertheless, this approach reduces the dimension-spreading factor, and thus the maximum achievable SIR_T also decreases.

The short effective duration of the MNWs reveals the multiple access capability of this modulation format. In contrast to conventional TDMA, this scheme is able to mitigate inter-system interferences in non-cooperative scenarios due to the context-aware nature of the MNWs. Under sensing errors, the parameters m_0 and M may not be equal at both inner nodes, yielding frequency errors and loss of orthogonality,

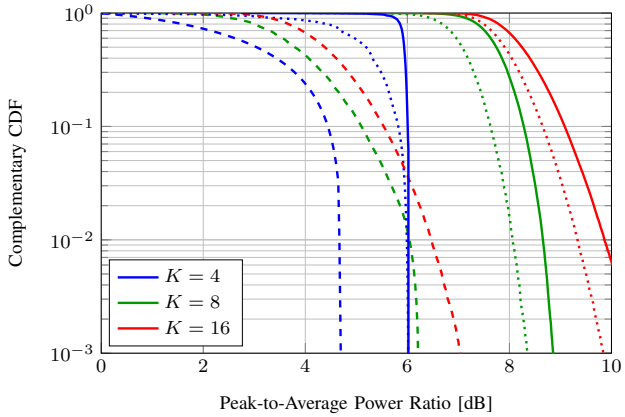

Fig. 8: CCDF of the minimum PAPR with QPSK symbols for different numbers of waveforms K. Solid lines are for OFDMA, dashed lines are for CS-TDMA (28) with $K = M$, and dotted lines are for the asymptotic MNWs (25) and (14) with $K = M$.

respectively, that can be reduced through synchronization schemes and subspace-matching methods (see, e.g., [44]).

Finally, yet importantly, note that MNWs are time-domain peaky signals. Even though their poor peak-to-average power ratio (PAPR), peaky signals in the time domain and spread over frequency can achieve the channel capacity in the limit of infinite bandwidth in some multipath channels (cf. [45] and references therein). Given the importance of PAPR for practical implementation, we evaluate in Figure 8 its complementary Cumulative Distribution Function (CDF), where the performance of Orthogonal Frequency-Division Multiple-Access (OFDMA) has been included as reference[5]. Despite OFDMA requires end-to-end calibration, and thus it is not appropriate in feedforward scenarios, we have considered OFDMA as a reference since it is a potential alternative in co-operative opportunistic communications. Figure 8 shows that, in the general case (non-consecutive DoF), MNWs present a slightly better PAPR than OFDMA. However, when the available DoF are consecutive, the CS-TDMA scheme exhibits a very competitive behavior in front of OFDMA, given the particular structure of the multiplex.

B. Transmission in Frequency-Selective Channels

This subsection[6] studies the feasibility of employing the MNWs (14) in frequency-selective (FS) channels. Since, as per Proposition 7, the MNWs-based transmission scheme asymptotically relies on Fourier matrices, we resort to the common multi-carrier strategy [46], that is, using a cyclic prefix (CP) at the transmitter and a one-tap frequency-domain equalizer at the receiver.

Accordingly, the transmitted signal is extended using a classic CP, that is, $\boldsymbol{x} = \left[\begin{array}{c:c} \tilde{\boldsymbol{x}}_{\text{CP}}^T & \tilde{\boldsymbol{x}}^T \end{array}\right]^T$, such that $\tilde{\boldsymbol{x}}_{\text{CP}}$ contains the last $N_{\text{CP}} \geq L_h - 1$ samples of the N-length signal $\tilde{\boldsymbol{x}}$, being L_h the length of the channel response. In order to take into account the impact of the CP on the waveform design, the asymptotically optimal sensing basis $\boldsymbol{U} = \boldsymbol{F}^H$ has to be replaced[7] by a structured $(N_{\text{CP}}+N)\times N$ non-orthogonal basis $\widetilde{\boldsymbol{U}} = \left[\begin{array}{c:c} \boldsymbol{U}_{\text{CP}}^T & \boldsymbol{U}^T \end{array}\right]^T$, where $\boldsymbol{U}_{\text{CP}}$ contains the last N_{CP} rows of $\boldsymbol{U}$. Therefore, the transmission matrix $\boldsymbol{\Phi} = [\boldsymbol{\phi}_0, \ldots, \boldsymbol{\phi}_{K-1}]$ is now given by

$$\boldsymbol{\Phi} = \left[\begin{array}{c} \widetilde{\boldsymbol{\Phi}}_{\text{CP}} \\ \hdashline \widetilde{\boldsymbol{\Phi}} \end{array}\right] = \widetilde{\boldsymbol{U}}_{\mathcal{N}}\boldsymbol{\Lambda} = \left[\begin{array}{c} \boldsymbol{U}_{\mathcal{N},\text{CP}} \\ \hdashline \boldsymbol{U}_{\mathcal{N}} \end{array}\right]\boldsymbol{\Lambda} \in \mathbb{C}^{(N_{\text{CP}}+N)\times K}, \tag{29}$$

where $\widetilde{\boldsymbol{\Phi}}_{\text{CP}}$ contains the last N_{CP} rows of $\widetilde{\boldsymbol{\Phi}} = \boldsymbol{U}_{\mathcal{N}}\boldsymbol{\Lambda} \in \mathbb{C}^{N\times K}$, $\widetilde{\boldsymbol{U}}_{\mathcal{N}} \in \mathbb{C}^{(N_{\text{CP}}+N)\times M}$ is the sensed null-space basis from $\widetilde{\boldsymbol{U}}$, $\boldsymbol{\Lambda} = [\boldsymbol{\lambda}_0, \ldots, \boldsymbol{\lambda}_{K-1}] \in \mathbb{C}^{M\times K}$ contains the linear combination coefficients vectors that define $\widetilde{\boldsymbol{\Phi}}$, and $\boldsymbol{U}_{\mathcal{N},\text{CP}}$ contains the last N_{CP} rows of $\boldsymbol{U}_{\mathcal{N}}$. Under these considerations, the extended transmitted signal is given by $\boldsymbol{x} = \boldsymbol{\Phi}\boldsymbol{a}$, where $\boldsymbol{a}$ contains the K transmitted symbols.

After removing the CP, the received signal is given by $\tilde{\boldsymbol{y}} = \boldsymbol{H}_{\text{II}}\tilde{\boldsymbol{x}} + \boldsymbol{w} + \boldsymbol{i} = \boldsymbol{F}^H\boldsymbol{\Sigma}_h\boldsymbol{F}\widetilde{\boldsymbol{\Phi}}\boldsymbol{a} + \boldsymbol{w} + \boldsymbol{i}$, where $\boldsymbol{w}$ and $\boldsymbol{i}$ stand for the noise and interferences, and $\boldsymbol{H}_{\text{II}} = \boldsymbol{F}^H\boldsymbol{\Sigma}_h\boldsymbol{F}$ is the $N\times N$ circulant inner channel matrix, with the diagonal matrix $\boldsymbol{\Sigma}_h$ containing the channel frequency response. Defining $\widetilde{\boldsymbol{\Phi}} = \boldsymbol{U}_{\mathcal{N}}\boldsymbol{\Lambda} \in \mathbb{C}^{N\times K}$, the received signal reads as

$$\begin{aligned}\tilde{\boldsymbol{y}} &= \boldsymbol{F}^H\left[\begin{array}{cc} \boldsymbol{\Sigma}_{\mathcal{S},h} & \boldsymbol{0} \\ \boldsymbol{0} & \boldsymbol{\Sigma}_{\mathcal{N},h} \end{array}\right]\left[\begin{array}{c} \boldsymbol{0}_{(N-M)\times M} \\ \hdashline \boldsymbol{I}_M \end{array}\right]\boldsymbol{\Lambda}\boldsymbol{a} + \boldsymbol{w} + \boldsymbol{i} \\ &= \boldsymbol{F}^H\left[\begin{array}{c} \boldsymbol{0}_{(N-M)\times M} \\ \hdashline \boldsymbol{\Sigma}_{\mathcal{N},h} \end{array}\right]\boldsymbol{\Lambda}\boldsymbol{a} + \boldsymbol{w} + \boldsymbol{i}.\end{aligned} \tag{30}$$

Note that (29) is steering the opportunistic information through the sensed null-space *eigenchannels* $\boldsymbol{\Sigma}_{\mathcal{N},h}$, minimizing the induced worst-case inter-system interference per DoF. In order to counteract the impact of the null-space *eigenchannels*, the inner receiver can implement a frequency-domain one-tap equalizer. As it is very well-known, different equalization criteria have been developed for this important problem (see, e.g., [47]), being this classical discussion out of the scope of this paper. In the sequel, in order to illustrate the feasibility of using this modulation format in FS channels, the zero-forcing equalizer depicted in Figure 9 is adopted, despite not being statistically optimal. In this sense, let us consider the zero-forcing matrix $\boldsymbol{G} = \boldsymbol{U}_{\mathcal{N}}\boldsymbol{\Sigma}_{\mathcal{N},h}^{-1}\boldsymbol{U}_{\mathcal{N}}^H$, such that $\tilde{\boldsymbol{\nu}} = \boldsymbol{G}\tilde{\boldsymbol{y}} = \boldsymbol{U}_{\mathcal{N}}\boldsymbol{\Lambda}\boldsymbol{a} + \boldsymbol{G}\boldsymbol{w} = \boldsymbol{\Psi}\boldsymbol{a} + \tilde{\boldsymbol{n}}$, being $\boldsymbol{\Psi} = \boldsymbol{U}_{\mathcal{N}}\boldsymbol{\Lambda} \in \mathbb{C}^{N\times K}$ the receiving opportunistic matrix. Since the transmission scheme in (29) combines the M carriers in $\widetilde{\boldsymbol{U}}_{\mathcal{N}}$ to design K waveforms that are orthogonal after removing the CP, the statistic for symbol decoding is given by $\boldsymbol{z} = \boldsymbol{\Psi}^H\tilde{\boldsymbol{\nu}} = \gamma\boldsymbol{a} + \boldsymbol{\Psi}\tilde{\boldsymbol{n}}$, where $\gamma < 1$ is the energy loss factor due to the CP insertion. In contrast to OFDMA, (29) performs time multiplexing, even though frequency multiplexing is also possible by tuning the basis $\widetilde{\boldsymbol{U}}_{\mathcal{N}}$ at the expense of increasing the persistent low interference density per DoF imposed on outer nodes.

[5]In this numerical example, we have not used any PAPR reduction technique, and the simulation was run considering the *native* version of both modulation schemes.

[6]For the sake of simplicity, we assume in this subsection the ideal case where both inner nodes identify the same null space, thus omitting the positioning vectors $\boldsymbol{r}_{\text{T}}$ and $\boldsymbol{r}_{\text{R}}$. Therefore, Proposition 5 holds. The realistic case accounting for inter-node subspace uncertainty is straightforward at expense of notational complexity.

[7]If the outer-network nodes employ a block transmission with N_{CP} guard symbols, as OFDMA, and the inner nodes are aware of this information, this step is not necessary whenever the guard symbols are removed before inferring the null space.

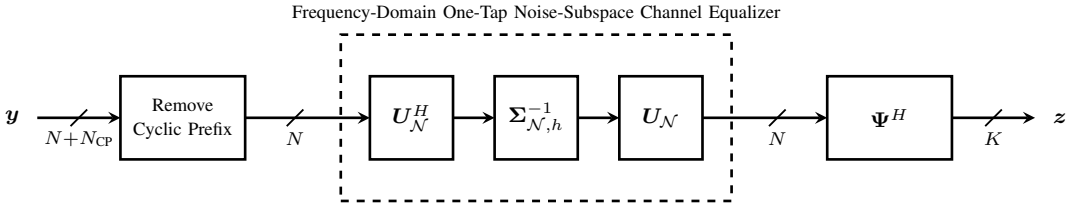

Fig. 9: Adopted opportunistic receiving scheme in FS channels.

V. Conclusions

This paper has studied a decentralized transmitting-receiving scheme for feedforward opportunistic communications, focusing on the context of asynchronous non-cooperative communications systems. A general study of the worst-case SIR optimization problem has been addressed through the MNTLS criterion. It has been shown that this criterion designs waveforms enjoying minimum induced interference and robust detection invariance properties, which are of paramount importance to guarantee coherent waveform detection despite the ambiguities of the asynchronous sensed available DoF. The solutions provide a per-waveform asynchronous sensing-basis DoF spreading. In other words, the structure of the residual inter-system interference is spread out, decreasing the outage induced on outer network nodes and maximizing the achievable SIDR. Since each involved waveform spans only one invariant DoF, the proposed solution becomes optimal in terms of finally occupied DoF. When the number of available DoF becomes asymptotically large, the studied scheme behaves as an efficient time-multiplexing modulation, denoted as CS-TDMA, which is optimal under mild operating conditions. Theoretical approximated models have been provided and numerically validated.

In this paper, the proposed waveform design scheme relies on the locally sensed null space, that is, on strict local sensing information. Interesting future extensions of this work may include the use of the additional knowledge given by the degree of confidence of the sensing information in order to provide an enhanced interference mitigation performance and cooperation between inner nodes.

Appendix A

Recalling (12a)–(12d), note that this proof is twofold. First, we address the maximization step, i.e.

$$\boldsymbol{E}_{\mathcal{N}} = \underset{\boldsymbol{E}_{\mathcal{N}}}{\arg\max} \sum_{k=0}^{K-1} \left\| \boldsymbol{E}_{\mathcal{N}}^H \boldsymbol{\phi}_k \right\|^2 \text{ s.t. } \|\boldsymbol{E}_{\mathcal{N}}\|_{\mathrm{F}}^2 \leq \xi^2. \quad (31)$$

Following a Lagrange multiplier approach, the solution to this quadratic problem leads to $\sum_{k=0}^{K-1} \boldsymbol{\phi}_k \boldsymbol{\phi}_k^H \boldsymbol{E}_{\mathcal{N}} = \mu \boldsymbol{E}_{\mathcal{N}}$, where μ is the Lagrange multiplier. Thus, the worst-case error matrix $\boldsymbol{E}_{\mathcal{N}}$ must be a rank-K matrix belonging to the subspace spanned by all orthonormal waveforms $\boldsymbol{\phi}_k$, that is, $\boldsymbol{E}_{\mathcal{N}} \in \langle [\boldsymbol{\phi}_0\ \boldsymbol{\phi}_1 \dots \boldsymbol{\phi}_{K-1}] \rangle$. Thus, even though ξ^2 is an unknown parameter, the solution to (31) discloses that in the worst case $\xi^2 = K$. This solution leads to the case where each orthonormal waveform $\boldsymbol{\phi}_k$ focuses all its energy on a single erroneous DoF. Taking into account this case and letting $\boldsymbol{E}_{\mathcal{N}} = [\boldsymbol{\phi}_0, \dots, \boldsymbol{\phi}_{K-1}]$, the minimization step in (12a) now reads as

$$\{\boldsymbol{\lambda}_k\}_{0\leq k\leq K-1} = \underset{\{\boldsymbol{\lambda}_k; \boldsymbol{e}_k\}}{\arg\min} \sum_{k=0}^{K-1} \left\| \widehat{\boldsymbol{U}}_{\mathcal{N}} \boldsymbol{\lambda}_k \right\|^2 \quad (32a)$$

$$\text{subject to} \quad \boldsymbol{\lambda}_k^H \widehat{\boldsymbol{U}}_{\mathcal{N}}^H \boldsymbol{e}_k = \alpha_k \quad (32b)$$

$$\boldsymbol{\lambda}_k^H \boldsymbol{\lambda}_{k'} = 0,\ k \neq k' \quad (32c)$$

which becomes a classic minimum-norm problem. Note that $\boldsymbol{e}_k$ is given in (13). For ease of notation, since α_k can be any positive real number, we consider an α_k such that $\|\boldsymbol{\phi}_k\|^2 = \|\boldsymbol{\lambda}_k\|^2 = 1$. The corresponding Lagrangian for this problem is given by

$$\mathcal{L}\left(\{\boldsymbol{\lambda}_k\}, \{\gamma_k\}, \{\eta_{kk'}\}\right) = \sum_{k=0}^{K-1} \boldsymbol{\lambda}_k^H \boldsymbol{\lambda}_k - \sum_{k=0}^{K-1} \gamma_k \left[\boldsymbol{\lambda}_k^H \widehat{\boldsymbol{U}}_{\mathcal{N}}^H \boldsymbol{e}_k - \alpha_k \right] - \sum_{k'=0}^{K-1} \sum_{k=k'+1}^{K-1} \eta_{kk'} \boldsymbol{\lambda}_k^H \boldsymbol{\lambda}_{k'}, \quad (33)$$

where $\{\gamma_k\}$ and $\{\eta_{kk'}\}$ are the Lagrange multipliers. Equating the gradient of (33) with respect to $\boldsymbol{\lambda}_k^H$ to zero, we get

$$\boldsymbol{\lambda}_k = \gamma_k \widehat{\boldsymbol{U}}_{\mathcal{N}}^H \boldsymbol{e}_k + \sum_{k'=0}^{k-1} \eta_{kk'} \boldsymbol{\lambda}_{k'}. \quad (34)$$

Plugging (34) into (32c), we obtain for $k' < k$

$$\boldsymbol{\lambda}_k^H \boldsymbol{\lambda}_i = \gamma_k^* \boldsymbol{e}_k^T \widehat{\boldsymbol{U}}_{\mathcal{N}} \boldsymbol{\lambda}_i + \sum_{k'=0}^{k-1} \eta_{ik'}^* \boldsymbol{\lambda}_{k'}^H \boldsymbol{\lambda}_i = \gamma_k^* \boldsymbol{e}_k^T \widehat{\boldsymbol{U}}_{\mathcal{N}} \boldsymbol{\lambda}_{k'} + \eta_{kk'}^* = 0, \quad (35)$$

where the second equality follows from the orthogonality of the new waveform designed with respect to the previous ones. Solving for $\eta_{kk'}^*$, we get $\eta_{kk'}^* = -\gamma_k^* \boldsymbol{e}_k^T \widehat{\boldsymbol{U}}_{\mathcal{N}} \boldsymbol{\lambda}_{k'}$. Now, substituting $\eta_{kk'}^*$ into $\boldsymbol{\lambda}_k$, we have that

$$\boldsymbol{\lambda}_k = \gamma_k \left[\widehat{\boldsymbol{U}}_{\mathcal{N}}^H \boldsymbol{e}_k - \sum_{k'=0}^{k-1} \boldsymbol{\lambda}_{k'} \left(\boldsymbol{e}_k^T \widehat{\boldsymbol{U}}_{\mathcal{N}} \boldsymbol{\lambda}_{k'} \right)^* \right] = \gamma_k \left[\widehat{\boldsymbol{U}}_{\mathcal{N}}^H \boldsymbol{e}_k - \sum_{k'=0}^{k-1} \boldsymbol{\lambda}_{k'} \boldsymbol{\lambda}_{k'}^H \widehat{\boldsymbol{U}}_{\mathcal{N}}^H \boldsymbol{e}_k \right], \quad (36)$$

and using (36) into (5), we obtain

$$\boldsymbol{\phi}_k = \gamma_k \widehat{\boldsymbol{P}}_0 \left[\boldsymbol{I}_N - \sum_{k'=0}^{k-1} \boldsymbol{\phi}_{k'} \boldsymbol{\phi}_{k'}^H \right] \boldsymbol{e}_k = \gamma_k \widehat{\boldsymbol{P}}_k \boldsymbol{e}_k, \quad (37)$$

which follows noting that $\widehat{\boldsymbol{P}}_0 = \widehat{\boldsymbol{U}}_{\mathcal{N}} \widehat{\boldsymbol{U}}_{\mathcal{N}}^H$. Concerning γ_k, plugging (37) into (32b), we get $\gamma_k = \alpha_k \left(\boldsymbol{e}_k^T \widehat{\boldsymbol{P}}_k \boldsymbol{e}_k \right)^{-1}$, which

$$(\mathrm{SIR}_\mathrm{T}+1)^{-1}=\frac{1}{K}\sum_{k=0}^{K-1}\frac{\boldsymbol{e}_k^T\widehat{\boldsymbol{P}}_0\left(\boldsymbol{I}_N-\sum_{i=0}^{k-1}\boldsymbol{\phi}_i\boldsymbol{\phi}_i^H\right)\widehat{\boldsymbol{P}}_{\mathcal{E}}\widehat{\boldsymbol{P}}_0\left(\boldsymbol{I}_N-\sum_{i=0}^{k-1}\boldsymbol{\phi}_i\boldsymbol{\phi}_i^H\right)\boldsymbol{e}_k}{\boldsymbol{e}_k^T\widehat{\boldsymbol{P}}_k\boldsymbol{e}_k} \tag{42}$$

$$\boldsymbol{e}_k^T\widehat{\boldsymbol{P}}_0\widehat{\boldsymbol{P}}_{\mathcal{E}}\widehat{\boldsymbol{P}}_0\boldsymbol{e}_k-2\boldsymbol{e}_k^T\widehat{\boldsymbol{P}}_0\widehat{\boldsymbol{P}}_{\mathcal{E}}\widehat{\boldsymbol{P}}_0\sum_{i=0}^{k-1}\boldsymbol{\phi}_i\boldsymbol{\phi}_i^H\boldsymbol{e}_k+\boldsymbol{e}_k^T\widehat{\boldsymbol{P}}_0\sum_{i=0}^{k-1}\boldsymbol{\phi}_i\boldsymbol{\phi}_i^H\widehat{\boldsymbol{P}}_{\mathcal{E}}\widehat{\boldsymbol{P}}_0\sum_{i=0}^{k-1}\boldsymbol{\phi}_i\boldsymbol{\phi}_i^H\boldsymbol{e}_k \tag{43}$$

$$\left[\widehat{\boldsymbol{P}}_{\mathcal{E}}\right]_{nn}-2\boldsymbol{e}_k^T\widehat{\boldsymbol{P}}_{\mathcal{E}}\sum_{i=0}^{k-1}\boldsymbol{\phi}_i\boldsymbol{\phi}_i^H\boldsymbol{e}_k+\boldsymbol{e}_k^T\sum_{i=0}^{k-1}\boldsymbol{\phi}_i\boldsymbol{\phi}_i^H\widehat{\boldsymbol{P}}_{\mathcal{E}}\sum_{i=0}^{k-1}\boldsymbol{\phi}_i\boldsymbol{\phi}_i^H\boldsymbol{e}_k\triangleq f_k\left(\widehat{\boldsymbol{P}}_{\mathcal{E}}\right) \tag{44}$$

means that $\|\boldsymbol{\phi}_k\|^2=1$ requires $\alpha_k=\left(\boldsymbol{e}_k^T\widehat{\boldsymbol{P}}_k\boldsymbol{e}_k\right)^{1/2}$. Finally, there is a last step to describe which is the selection of the optimum linear prediction vector $\boldsymbol{e}_k=\left[\boldsymbol{0}_{n(k)-1}^T\ 1\ \boldsymbol{0}_{N-n(k)}^T\right]^T$. Substituting γ_k into (37), we note that the column of $\widehat{\boldsymbol{P}}_k$ including the maximum value of its main diagonal must be selected, i.e.,

$$n(k)=\underset{n\in\{1,\ldots,N\}}{\arg\max}\ \boldsymbol{e}_k^T\widehat{\boldsymbol{P}}_k\boldsymbol{e}_k=\underset{n\in\{1,\ldots,N\}}{\arg\max}\left[\widehat{\boldsymbol{P}}_k\right]_{nn}, \tag{38}$$

so that the designed waveform $\boldsymbol{\phi}_k$ meets the minimum-norm condition in (32a). In view of (37)–(38), the design of the K waveforms $\{\boldsymbol{\phi}_k\}_k$ can be tackled as in Algorithm 1.

APPENDIX B

From the definition of $(S_T/I_T)=\mathrm{SIR}_\mathrm{T}+1$ in (17), we note that in the minimization step

$$\begin{aligned}\boldsymbol{E}_{\mathcal{N}}&=\underset{\boldsymbol{E}_{\mathcal{N}}}{\arg\min}\ \frac{\sum_{k=0}^{K-1}\|\boldsymbol{\phi}_k\|^2}{\sum_{k=0}^{K-1}\left\|\boldsymbol{E}_{\mathcal{N}}^H\boldsymbol{\phi}_k\right\|^2}\\&=\underset{\boldsymbol{E}_{\mathcal{N}}}{\arg\min}\ \frac{\|\boldsymbol{\Phi}\|_\mathrm{F}^2}{\left\|\boldsymbol{E}_{\mathcal{N}}^H\boldsymbol{\Phi}\right\|_\mathrm{F}^2}\geq\frac{1}{\|\boldsymbol{E}_{\mathcal{N}}\|_\mathrm{F}^2}\geq\frac{1}{\xi^2},\end{aligned} \tag{39}$$

where we make use of the Cauchy-Schwarz inequality. Thus, from (39), we see that $\boldsymbol{E}_{\mathcal{N}}$ must be a rank-K matrix belonging to $\langle[\boldsymbol{\phi}_0\ \boldsymbol{\phi}_1\ldots\boldsymbol{\phi}_{K-1}]\rangle$ as discussed in Appendix A, and hence the criterion in (17) becomes the same MNTLS criterion given in (12a). Note that the lower-bound in (39) represents a lower-bound on the ratio S_T/I_T. Nonetheless, a more accurate study is required to prove (18). Recalling (11), we note that

$$\mathrm{SIR}_\mathrm{T}+1=\frac{S_T}{I_T}=\frac{\sum_{k=0}^{K-1}\|\boldsymbol{\phi}_k\|^2}{\sum_{k=0}^{K-1}\|\boldsymbol{E}_{\mathcal{N}}^H\boldsymbol{\phi}_k\|^2}=\frac{K}{\sum_{k=0}^{K-1}\boldsymbol{\phi}_k^H\widehat{\boldsymbol{P}}_{\mathcal{E}}\boldsymbol{\phi}_k}, \tag{40}$$

where $\widehat{\boldsymbol{P}}_{\mathcal{E}}=\boldsymbol{E}_{\mathcal{N}}\boldsymbol{E}_{\mathcal{N}}^H$ is the unknown projector onto the subspace spanned by the unknown sensing error matrix $\widehat{\boldsymbol{E}}_{\mathcal{N}}$. The last equality in (40) follows from recalling that $\|\boldsymbol{\phi}_k\|^2=1$, for $k=0,\ldots,K-1$. Using the expression for $\boldsymbol{\phi}_k$ given in (14) and $\boldsymbol{e}_k$ defined in (13), observe that

$$\begin{aligned}(\mathrm{SIR}_\mathrm{T}+1)^{-1}&=\frac{1}{K}\sum_{k=0}^{K-1}\frac{\boldsymbol{e}_k^T\widehat{\boldsymbol{P}}_k\widehat{\boldsymbol{P}}_{\mathcal{E}}\widehat{\boldsymbol{P}}_k\boldsymbol{e}_k}{\boldsymbol{e}_k^T\widehat{\boldsymbol{P}}_k\boldsymbol{e}_k}=\\&\frac{1}{K}\sum_{k=0}^{K-1}(\mathrm{SIR}_k+1)^{-1},\end{aligned} \tag{41}$$

i.e. (40) is the harmonic mean of $\{(\mathrm{SIR}_k+1)\}_{0\leq k\leq K-1}$. Plugging the definition of $\widehat{\boldsymbol{P}}_k$ given in (37) into (41) leads to (42) on the top of this page.

Note that the denominator in (42) is just the n-th diagonal element of matrix $\widehat{\boldsymbol{P}}_k$, i.e. $\left[\widehat{\boldsymbol{P}}_k\right]_{nn}$. Regarding the numerator, it can be expanded as in (43), where the second term follows from the Hermitian property of orthogonal projectors. Recalling that $\widehat{\boldsymbol{P}}_0=\widehat{\boldsymbol{U}}_{\mathcal{N}}\widehat{\boldsymbol{U}}_{\mathcal{N}}^H$, and $\boldsymbol{E}_{\mathcal{N}}$ is a subset of columns of $\widehat{\boldsymbol{U}}_{\mathcal{N}}$, note that $\widehat{\boldsymbol{P}}_0\widehat{\boldsymbol{P}}_{\mathcal{E}}=\widehat{\boldsymbol{P}}_{\mathcal{E}}$. Therefore, (43) can be simplified as in (44), where $\left[\widehat{\boldsymbol{P}}_{\mathcal{E}}\right]_{nn}$ is the n-th diagonal element of matrix $\widehat{\boldsymbol{P}}_{\mathcal{E}}$. Since (44) does not depend on $\widehat{\boldsymbol{P}}_k$, it can be identified as a function of the waveform index k and $\widehat{\boldsymbol{P}}_{\mathcal{E}}$. Finally, (40) leads to

$$\mathrm{SIR}_\mathrm{T}(\boldsymbol{E}_{\mathcal{N}};\boldsymbol{\lambda}_k)+1=\frac{K}{\sum_{k=0}^{K-1}\left(f_k\left(\widehat{\boldsymbol{P}}_{\mathcal{E}}\right)/\left[\widehat{\boldsymbol{P}}_k\right]_{nn}\right)}. \tag{44}$$

APPENDIX C

Recalling the definition of the SIDR_T in (19), notice that $\mathrm{SIDR}_\mathrm{T}=N_E\cdot\mathrm{SIR}_\mathrm{T}$ and thus, it is proportional to (42). Studying $f_k\left(\widehat{\boldsymbol{P}}_{\mathcal{E}}\right)$ in (44) and $\left[\widehat{\boldsymbol{P}}_k\right]_{nn}$, they can be written for $k\neq k'$ as

$$f_k\left(\widehat{\boldsymbol{P}}_{\mathcal{E}}\right)=\left[\widehat{\boldsymbol{P}}_{\mathcal{E}}\right]_{nn}+\delta_{k,k'}^{(1)}, \tag{45a}$$

$$\left[\widehat{\boldsymbol{P}}_k\right]_{nn}=\left[\widehat{\boldsymbol{P}}_0\right]_{nn}+\delta_{k,k'}^{(2)}, \tag{45b}$$

where $\delta_{k,k'}^{(1)}$ and $\delta_{k,k'}^{(2)}$ are second-order terms that depend on off-diagonal elements of the involved projectors. As for [48], off-diagonal entries of spectral projectors become asymptotically irrelevant in comparison with the main diagonal entries. Therefore, letting $\delta_{k,k'}^{(1)},\delta_{k,k'}^{(2)}\to 0$, note that $f_k\left(\widehat{\boldsymbol{P}}_{\mathcal{E}}\right)\approx\boldsymbol{e}_k^T\widehat{\boldsymbol{P}}_{\mathcal{E}}\boldsymbol{e}_k$ and $\left[\widehat{\boldsymbol{P}}_k\right]_{nn}\approx\boldsymbol{e}_k^T\widehat{\boldsymbol{P}}_0\boldsymbol{e}_k$. Thus, for $N\to\infty$ and $M=\mathrm{rank}\left[\widehat{\boldsymbol{U}}_{\mathcal{N}}\right]\gg 1$, the SIDR_T can be well-approximated as

$$\begin{aligned}\mathrm{SIDR}_\mathrm{T}(\boldsymbol{E}_{\mathcal{N}};\boldsymbol{\lambda}_k)&\approx\frac{K-\sum_{k=0}^{K-1}\left[\widehat{\boldsymbol{P}}_{\mathcal{E}}\right]_{nn}\left[\widehat{\boldsymbol{P}}_0\right]_{nn}^{-1}}{\frac{1}{N_E}\sum_{k=0}^{K-1}\left[\widehat{\boldsymbol{P}}_{\mathcal{E}}\right]_{nn}\left[\widehat{\boldsymbol{P}}_0\right]_{nn}^{-1}}=\\&N\cdot\frac{M}{N}\cdot\left(1-\frac{N_E}{M}\right),\end{aligned} \tag{46}$$

where the last equality can be shown from the asymptotic eigendecomposition of an autocorrelation matrix [43]. In this sense, all the diagonal elements of the two involved projection matrices are constant and given by $[\widehat{\boldsymbol{P}}_0]_{nn} = M/N$ and $[\widehat{\boldsymbol{P}}_{\mathcal{E}}]_{nn} = N_E/N$, leading to (46).

APPENDIX D

Recall that $\boldsymbol{\phi}_k = \widehat{\boldsymbol{U}}_{\mathcal{N}}\boldsymbol{\lambda}_k$, where $\boldsymbol{\lambda}_k$ is as in (36). The energy allocated to each DoF sensed as available is given in the main diagonal of the matrix $\widehat{\boldsymbol{U}}_{\mathcal{N}}^H\boldsymbol{\phi}_k\boldsymbol{\phi}_k^H\widehat{\boldsymbol{U}}_{\mathcal{N}} = \boldsymbol{\lambda}_k\boldsymbol{\lambda}_k^H$. For ease of notation, (36) can be simplified, by inspection, as

$$\begin{aligned}\boldsymbol{\lambda}_k = \gamma_k\left[\widehat{\boldsymbol{U}}_{\mathcal{N}}^H\boldsymbol{e}_k - \sum_{k'=0}^{k-1}\boldsymbol{\lambda}_{k'}\boldsymbol{\lambda}_{k'}^H\widehat{\boldsymbol{U}}_{\mathcal{N}}^H\boldsymbol{e}_k\right] = \\ \gamma_k\widehat{\boldsymbol{U}}_{\mathcal{N}}^H\left[\boldsymbol{e}_k - \sum_{k'=0}^{k-1}\beta_{k'}\boldsymbol{e}_{k'}\right],\end{aligned} \tag{47}$$

where $\beta_{k'} \triangleq f\left(\gamma_{k'}, [\boldsymbol{P}_0]_{kk'}, [\boldsymbol{P}_0]_{ik'}\right)$, for $0 \le i \le k'-1$, and $\boldsymbol{e}_k$ is given in (13). Thus, for $i = 1, \ldots, \operatorname{rank}\left[\widehat{\boldsymbol{U}}_{\mathcal{N}}\right]$, we have that

$$\begin{aligned}\left[\boldsymbol{\lambda}_k\boldsymbol{\lambda}_k^H\right]_{ii} = |\gamma_k|^2\Bigg[\left[\widehat{\boldsymbol{U}}_{\mathcal{N}}^H\boldsymbol{e}_k\boldsymbol{e}_k^T\widehat{\boldsymbol{U}}_{\mathcal{N}}\right]_{ii} + \\ \sum_{k'=0}^{k-1}\beta_{k'}^2\left[\widehat{\boldsymbol{U}}_{\mathcal{N}}^H\boldsymbol{e}_{k'}\boldsymbol{e}_{k'}^T\widehat{\boldsymbol{U}}_{\mathcal{N}}\right]_{ii}\Bigg],\end{aligned} \tag{48}$$

which follows from noting that $\operatorname{diag}\left[\boldsymbol{e}_k\boldsymbol{e}_{k'}^T\right] = \boldsymbol{0}_{N\times 1}$ for $k \neq k'$. Since $\boldsymbol{e}_k$ is a sparse vector with a non-null entry (equal to one) at position $n(k)$, it is easy to check that $\widehat{\boldsymbol{U}}_{\mathcal{N}}^H\boldsymbol{e}_k$ is the $n(k)$-th column of $\widehat{\boldsymbol{U}}_{\mathcal{N}}^H$, which is denoted by $\boldsymbol{u}_{n(k)}$. As $\left[\boldsymbol{u}_{n(k)}\boldsymbol{u}_{n(k)}^H\right]_{ii} = \left|\left[\boldsymbol{u}_{n(k)}\right]_i\right|^2$, (48) yields

$$\left[\boldsymbol{\lambda}_k\boldsymbol{\lambda}_k^H\right]_{ii} = |\gamma_k|^2\left[\left|\left[\boldsymbol{u}_{n(k)}\right]_i\right|^2 + \sum_{k'=0}^{k-1}\beta_{k'}^2\left|\left[\boldsymbol{u}_{n(k')}\right]_i\right|^2\right]. \tag{49}$$

Note that, in general, $\left|\left[\boldsymbol{u}_{n(k)}\right]_i\right| \neq \left|\left[\boldsymbol{u}_{n(k)}\right]_j\right|$ for $i \neq j$, and hence the energy is not uniformly distributed. However, the asymptotic eigendecomposition of autocorrelation matrices [43] reveals that

$$\operatorname{diag}\left[\boldsymbol{\lambda}_k\boldsymbol{\lambda}_k^H\right] \xrightarrow[N\to\infty]{} |\gamma_k|^2\left[1 + \sum_{k'=0}^{k-1}\beta_{k'}^2\right]\boldsymbol{1}_{N\times 1}, \tag{50}$$

and thus the MNTLS solution is asymptotically providing a *uniform* per-DoF energy distribution.

APPENDIX E

The subspace-mismatch energy loss when $K = 1$ waveform is transmitted is given by

$$\Gamma_1 = \frac{\boldsymbol{\phi}_0^H\boldsymbol{\phi}_0}{|\boldsymbol{\psi}_0^H\boldsymbol{\phi}_0|^2} = \frac{\boldsymbol{e}_0^T\widehat{\boldsymbol{P}}_{0,\mathrm{R}}\boldsymbol{e}_0\boldsymbol{e}_0^T\widehat{\boldsymbol{P}}_{0,\mathrm{T}}\boldsymbol{e}_0}{(\boldsymbol{e}_0^T\widehat{\boldsymbol{P}}_{0,\mathrm{R}}\widehat{\boldsymbol{P}}_{0,\mathrm{T}}\boldsymbol{e}_0)^2}, \tag{51}$$

which follows from noting that $\|\boldsymbol{\phi}\|^2 = 1$, and recalling that $\boldsymbol{\phi}_0 = (\boldsymbol{e}_0^T\widehat{\boldsymbol{P}}_{0,\mathrm{T}}\boldsymbol{e}_0)^{-1/2}\widehat{\boldsymbol{P}}_{0,\mathrm{T}}\boldsymbol{e}_0$ and $\boldsymbol{\psi}_0 = (\boldsymbol{e}_0^T\widehat{\boldsymbol{P}}_{0,\mathrm{R}}\boldsymbol{e}_0)^{-1/2}\widehat{\boldsymbol{P}}_{0,\mathrm{R}}\boldsymbol{e}_0$, being $\widehat{\boldsymbol{P}}_{0,\mathrm{T}}$ and $\widehat{\boldsymbol{P}}_{0,\mathrm{R}}$ the orthogonal projectors onto $\widehat{\mathcal{N}}_{\mathrm{T}} = \left\langle\widehat{\boldsymbol{U}}_{\mathcal{N}}(\boldsymbol{r}_{\mathrm{T}})\right\rangle$ and $\widehat{\mathcal{N}}_{\mathrm{R}} = \left\langle\widehat{\boldsymbol{U}}_{\mathcal{N}}(\boldsymbol{r}_{\mathrm{R}})\right\rangle$, respectively. Under subspace mismatch, that is $\widehat{\mathcal{N}}_{\mathrm{T}} \neq \widehat{\mathcal{N}}_{\mathrm{R}}$, these subspaces can be decomposed as $\widehat{\mathcal{N}}_{\mathrm{T}} = \mathcal{N}_0 \oplus \mathcal{E}_{\mathrm{T}}$ and $\widehat{\mathcal{N}}_{\mathrm{R}} = \mathcal{N}_0 \oplus \mathcal{E}_{\mathrm{R}}$, where $\mathcal{N}_0 = \widehat{\mathcal{N}}_{\mathrm{T}} \cap \widehat{\mathcal{N}}_{\mathrm{R}}$, and $\mathcal{E}_{\mathrm{T}}$ and $\mathcal{E}_{\mathrm{R}}$ stand for the noise-subspace excess with respect to $\mathcal{N}_0$ at inner transmitter and receiver, respectively. Since $\mathcal{E}_{\mathrm{T}} \cap \mathcal{E}_{\mathrm{R}} = \emptyset$, the orthogonal projectors are given by $\widehat{\boldsymbol{P}}_{0,\mathrm{T}} = \boldsymbol{P}_{\mathcal{N}_0} + \boldsymbol{P}_{\mathcal{E}_{\mathrm{T}}}$ and $\widehat{\boldsymbol{P}}_{0,\mathrm{R}} = \boldsymbol{P}_{\mathcal{N}_0} + \boldsymbol{P}_{\mathcal{E}_{\mathrm{R}}}$. Thus, (51) leads to

$$\Gamma_1 = \frac{\boldsymbol{e}_0^T(\boldsymbol{P}_{\mathcal{N}_0} + \boldsymbol{P}_{\mathcal{E}_{\mathrm{R}}})\boldsymbol{e}_0\boldsymbol{e}_0^T(\boldsymbol{P}_{\mathcal{N}_0} + \boldsymbol{P}_{\mathcal{E}_{\mathrm{T}}})\boldsymbol{e}_0}{(\boldsymbol{e}_0^T\boldsymbol{P}_{\mathcal{N}_0}\boldsymbol{e}_0)^2}. \tag{52}$$

Taking into account the asymptotic eigendecomposition of any autocorrelation matrix [43], the involved projectors in (52) will asymptotically have a constant diagonal equal to $[\boldsymbol{P}_{\mathcal{N}_0}]_{nn} = M_0/N$, $[\boldsymbol{P}_{\mathcal{E}_{\mathrm{T}}}]_{nn} = \kappa_{\mathrm{T}}/N$ and $[\boldsymbol{P}_{\mathcal{E}_{\mathrm{R}}}]_{nn} = \kappa_{\mathrm{R}}/N$, where M_0, κ_{T} and κ_{R} are the dimensions of $\mathcal{N}_0$, $\mathcal{E}_{\mathrm{T}}$, and $\mathcal{E}_{\mathrm{R}}$, respectively. Therefore, defining $\rho_{\mathrm{T}} \triangleq \kappa_{\mathrm{T}}/M_0$ and $\rho_{\mathrm{R}} \triangleq \kappa_{\mathrm{R}}/M_0$, (52) yields

$$\Gamma_1 \xrightarrow[N\to\infty]{} \frac{(M_0+\kappa_{\mathrm{R}})(M_0+\kappa_{\mathrm{T}})}{M_0^2} = 1+\rho_{\mathrm{T}}+\rho_{\mathrm{R}}+\rho_{\mathrm{T}}\rho_{\mathrm{R}}. \tag{53}$$

REFERENCES

[1] J. Borras and G. Vazquez, "Decentralized shaping for pilot generation and detection in opportunistic communications," in *2019 IEEE Int. Conf. Commun. (ICC)*, May 2019, pp. 1–6.

[2] J. Borras and G. Vazquez, "Interference mitigation in opportunistic transmission under degrees-of-freedom sensing uncertainties," in *2019 IEEE Global Commun. Conf. (GLOBECOM)*, Dec 2019, pp. 1–6.

[3] X. Chen, D. W. K. Ng, W. Yu, E. G. Larsson, N. Al-Dhahir, and R. Schober, "Massive access for 5G and beyond," *IEEE J. Sel. Areas Commun.*, vol. 39, no. 3, pp. 615–637, 2021.

[4] H. Nikbakht, M. Wigger, and S. Shamai Shitz, "Coordinated multi-point transmission and reception for mixed-delay traffic," *IEEE Trans. Commun.*, vol. 69, no. 12, pp. 8116–8131, 2021.

[5] M. Sharif and B. Hassibi, "A comparison of time-sharing, DPC, and beamforming for MIMO broadcast channels with many users," *IEEE Trans. Commun.*, vol. 55, no. 1, pp. 11–15, 2007.

[6] V. R. Cadambe and S. A. Jafar, "Interference alignment and degrees of freedom of the k-user interference channel," *IEEE Trans. Inf. Theory*, vol. 54, no. 8, pp. 3425–3441, 2008.

[7] N. Zhao, F. R. Yu, M. Jin, Q. Yan, and V. C. M. Leung, "Interference alignment and its applications: A survey, research issues, and challenges," *IEEE Commun. Surveys Tut.*, vol. 18, no. 3, pp. 1779–1803, 2016.

[8] O. El Ayach, S. W. Peters, and R. W. Heath, "The practical challenges of interference alignment," *IEEE Wireless Commun.*, vol. 20, no. 1, pp. 35–42, 2013.

[9] M. Zohdy, A. Tajer, and S. Shamai, "Distributed interference management: A broadcast approach," *IEEE Trans. Commun.*, vol. 69, no. 1, pp. 149–163, 2021.

[10] A. Lozano, R. W. Heath, and J. G. Andrews, "Fundamental limits of cooperation," *IEEE Trans. Inf. Theory*, vol. 59, no. 9, pp. 5213–5226, 2013.

[11] P. Viswanath, D. N. C. Tse, and R. Laroia, "Opportunistic beamforming using dumb antennas," *IEEE Trans. Inf. Theory*, vol. 48, no. 6, pp. 1277–1294, Jun 2002.

[12] L. Lu, G. Y. Li, A. Maaref, and R. Yao, "Opportunistic transmission exploiting frequency- and spatial-domain degrees of freedom," *IEEE Wireless Commun.*, vol. 21, no. 2, pp. 91–97, Apr 2014.

[13] Z. Chen and M. Kountouris, "Decentralized opportunistic access for D2D underlaid cellular networks," *IEEE Trans. Commun.*, vol. 66, no. 10, pp. 4842–4853, 2018.

[14] X. Yi and H. Sun, "Opportunistic treating interference as noise," *IEEE Trans. Inf. Theory*, vol. 66, no. 1, pp. 520–533, 2020.

[15] A. Goldsmith, S. A. Jafar, I. Maric, and S. Srinivasa, "Breaking spectrum gridlock with cognitive radios: an information theoretic perspective," *Proc. IEEE*, vol. 97, no. 5, pp. 894–914, May 2009.

[16] A. Krishnamoorthy and R. Schober, "Downlink MIMO-RSMA with successive null-space precoding," *IEEE Trans. Wireless Commun.*, pp. 1–1, 2022.

[17] A. A. Esswie and K. I. Pedersen, "Null space based preemptive scheduling for joint URLLC and eMBB traffic in 5G networks," in *2018 IEEE Globecom Workshops (GC Wkshps)*, 2018, pp. 1–6.
[18] J. A. Mahal, A. Khawar, A. Abdelhadi, and T. C. Clancy, "Spectral coexistence of MIMO radar and MIMO cellular system," *IEEE Transactions on Aerospace and Electronic Systems*, vol. 53, no. 2, pp. 655–668, 2017.
[19] W. Fu, R. Yao, F. Gao, J. C. F. Li, and M. Lei, "Robust null-space based interference avoiding scheme for D2D communication underlaying cellular networks," in *2013 IEEE Wireless Commun. and Netw. Conf. (WCNC)*, 2013, pp. 4158–4162.
[20] S. M. Perlaza, N. Fawaz, S. Lasaulce, and M. Debbah, "From spectrum pooling to space pooling: opportunistic interference alignment in MIMO cognitive networks," *IEEE Trans. Signal Process.*, vol. 58, no. 7, pp. 3728–3741, Jul 2010.
[21] C. G. Tsinos and K. Berberidis, "Blind opportunistic interference alignment in MIMO cognitive radio systems," *IEEE J. Emerging Sel. Topics in Circuits and Systems*, vol. 3, no. 4, pp. 626–639, 2013.
[22] M. El-Absi, M. Shaat, F. Bader, and T. Kaiser, "Interference alignment with frequency-clustering for efficient resource allocation in cognitive radio networks," *IEEE Trans. Wireless Commun.*, vol. 14, no. 12, pp. 7070–7082, 2015.
[23] L. S. Cardoso, M. Kobayashi, F. R. P. Cavalcanti, and M. Debbah, "Vandermonde-subspace frequency division multiplexing for two-tiered cognitive radio networks," *IEEE Trans. Commun.*, vol. 61, no. 6, pp. 2212–2220, Jun 2013.
[24] W. Liu, Q. Feng, J. Pang, Q. Hu, R. Yin, and G. Yu, "Robust rate-maximization precoder design for VFDM system," *IEEE Trans. Veh. Technol.*, vol. 69, no. 3, pp. 2747–2757, 2020.
[25] Q. Feng, J. Pang, M. Maso, M. Debbah, and W. Tong, "IDFT-VFDM for supplementary uplink and LTE-NR co-existence," *IEEE Trans. Wireless Commun.*, vol. 19, no. 5, pp. 3435–3448, 2020.
[26] M. Maso, M. Debbah, and L. Vangelista, "A distributed approach to interference alignment in OFDM-based two-tiered networks," *IEEE Trans. Veh. Technol.*, vol. 62, no. 5, pp. 1935–1949, 2013.
[27] L. Lu, G. Y. Li, and A. Maaref, "Spatial-frequency signal alignment for opportunistic transmission," *IEEE Trans. Signal Process.*, vol. 62, no. 6, pp. 1561–1575, Mar 2014.
[28] L. Lu, G. Y. Li, and A. Maaref, "Nullspace releasing for spatial-frequency opportunistic transmission," *IEEE Commun. Lett.*, vol. 18, no. 10, pp. 1843–1846, 2014.
[29] Y. Noam and A. J. Goldsmith, "Blind null-space learning for MIMO underlay cognitive radio with primary user interference adaptation," *IEEE Trans. Wireless Commun.*, vol. 12, no. 4, pp. 1722–1734, 2013.
[30] J. Font-Segura, G. Vazquez, and J. Riba, "Single and multi-frequency wideband spectrum sensing with side-information," *IET Signal Process.*, vol. 8, no. 8, pp. 831–843, 2014.
[31] Y. Noam, A. Manolakos, and A. J. Goldsmith, "Null space learning with interference feedback for spatial division multiple access," *IEEE Trans. Wireless Commun.*, vol. 13, no. 10, pp. 5699–5715, 2014.
[32] A. Mariani, A. Giorgetti, and M. Chiani, "Wideband spectrum sensing by model order selection," *IEEE Trans. Wireless Commun.*, vol. 14, no. 12, pp. 6710–6721, Dec 2015.
[33] A. Ali and W. Hamouda, "Advances on spectrum sensing for cognitive radio networks: Theory and applications," *IEEE Commun. Surveys Tut.*, vol. 19, no. 2, pp. 1277–1304, Secondquarter 2017.
[34] M. Shaghaghi and S. A. Vorobyov, "Subspace leakage analysis and improved DOA estimation with small sample size," *IEEE Trans. Signal Process.*, vol. 63, no. 12, pp. 3251–3265, 2015.
[35] R. G. Gallager, *Information Theory and Reliable Communications*. John Wiley & Sons, 1968.
[36] D. Tse and P. Viswanath, *Fundamentals of Wireless Communication*. Cambridge University Press, 2005.
[37] D. Tufts and R. Kumaresan, "Singular value decomposition and improved frequency estimation using linear prediction," *IEEE Trans. Acoust., Speech, and Signal Process.*, vol. 30, no. 4, pp. 671–675, 1982.
[38] M. H. Al-Ali and K. C. Ho, "Transmit precoding in underlay MIMO cognitive radio with unavailable or imperfect knowledge of primary interference channel," *IEEE Trans. Wireless Commun.*, vol. 15, no. 8, pp. 5143–5155, Aug 2016.
[39] E. M. Dowling and R. D. DeGroat, "The equivalence of the total least squares and minimum norm methods," *IEEE Trans. Signal Process.*, vol. 39, no. 8, pp. 1891–1892, Aug 1991.
[40] S. V. Huffel and J. Vandewalle, *The Total Least Squares Problem*. Society for Industrial and Applied Mathematics, 1991.
[41] I. Markovsky and S. V. Huffel, "Overview of total least-squares methods," *Signal Process.*, vol. 87, no. 10, pp. 2283–2302, 2007.
[42] J. Borras and G. Vazquez, "Distributed feedback-aided subspace concurrent opportunistic communications," in *2019 IEEE 20th Int. Workshop Signal Process. Adv. Wireless Commun. (SPAWC)*, Jul 2019, pp. 1–5.
[43] R. M. Gray, *Toeplitz and circulant matrices: A review*. Now Publishers, 2006.
[44] M. Tschannen and H. Bölcskei, "Noisy subspace clustering via matching pursuits," *IEEE Trans. Inf. Theory*, vol. 64, no. 6, pp. 4081–4104, 2018.
[45] D. Porrat, "Information theory of wideband communications," *IEEE Commun. Surveys Tut.*, vol. 9, no. 2, pp. 2–16, 2007.
[46] Z. Wang and G. Giannakis, "Wireless multicarrier communications," *IEEE Signal Process. Mag.*, vol. 17, no. 3, pp. 29–48, 2000.
[47] A. Scaglione, G. Giannakis, and S. Barbarossa, "Redundant filterbank precoders and equalizers. i. unification and optimal designs," *IEEE Trans. Signal Process.*, vol. 47, no. 7, pp. 1988–2006, 1999.
[48] M. Benzi and V. Simoncini (eds.), *Exploiting hidden structure in matrix computations: Algorithms and applications*. Springer, 2016.

Jordi Borras (S'15, M'23) received the Bachelor's, Master's, and Ph.D. degrees in Telecommunication Engineering from the Technical University of Catalonia (UPC-BarcelonaTECH), Barcelona, Spain, in 2016, 2018, and 2023, respectively. He has been involved with the Signal Processing and Communications Research Group, Department of Signal Theory and Communications, UPC, since 2017; until January 2023 as a pre-doctoral researcher, and currently as a post-doctoral researcher. In June 2018, he was awarded a pre-doctoral fellowship (FPI) by the Spanish Ministry of Science and Innovation (National Plan for Scientific and Technical Research and Innovation). His research interests are Statistical Signal Processing, Digital Communications, and Information Theory, with particular emphasis on interference management. Dr. Borras has participated in research projects funded by the Spanish Government and the European Commission (VII Framework Program). He is a co-recipient of the Student Video Exposition Award of the 2020 IEEE International Symposium on Information Theory (ISIT).

Gregori Vazquez (SM'98) was born in Barcelona, Spain, in 1961. He received the M.Sc. and Ph.D. degrees in telecommunications engineering from the Technical University of Catalonia (UPC), BarcelonaTECH, in 1984 and 1988, respectively. He has been a Professor with the Department of Signal Theory and Communications, UPC, since 2000. His general interests are Statistical Signal and Data Processing and Digital Communications. In particular, he has been especially active in interference management and mitigation techniques. He has been involved in research projects in mobile, satellite, and wireless communications of the European Commission, of the European Space Agency, and for private companies. Dr. Vazquez is a recipient of the 2003 Best Paper Award of the IEEE Signal Processing Society, and the 2013 Best Paper Award of the IEEE International Conference on Communications (ICC). He was serving as the Program Director of the Research Program on Communications of Spain from 2004 to 2006. He was also serving in the Information and Communication Technologies Committee (ICTC) of the VII Framework Program of the European Union from 2007 to 2011. He served as a member of the Editorial Board of the IEEE SIGNAL PROCESSING MAGAZINE from 2002 to 2006, as an Associate Editor of the IEEE TRANSACTIONS ON SIGNAL PROCESSING from 1999 to 2005, as a member of the Signal Processing for Communications Technical Committee and the Signal Processing Theory and Methods Technical Committee.